

An Effective Model of the Retinoic Acid Induced HL-60 Differentiation Program

Ryan Tasseff, Holly A. Jensen, Johanna Congleton[†], Wei Dai, Katherine Rogers, Adithya Sagar, Rodica P. Bunaciu[†], Andrew Yen[†], and Jeffrey D. Varner*

Robert Frederick Smith School of Chemical and Biomolecular Engineering and [†]Department of Biomedical Sciences, Cornell University, Ithaca NY 14853

Running Title: Effective modeling of HL-60 differentiation

To be submitted: ?

*Corresponding author:

Jeffrey D. Varner,

Professor, Robert Frederick Smith School of Chemical and Biomolecular Engineering,
244 Olin Hall, Cornell University, Ithaca NY, 14853

Email: jdv27@cornell.edu

Phone: (607) 255 - 4258

Fax: (607) 255 - 9166

Abstract

In this study, we present an effective model All-Trans Retinoic Acid (ATRA)-induced differentiation of HL-60 cells. The model describes a key architectural feature of ATRA-induced differentiation, positive feedback between an ATRA-inducible signalsome complex involving many proteins including Vav1, a guanine nucleotide exchange factor, and the activation of the mitogen activated protein kinase (MAPK) cascade. The model, which was developed by integrating logical rules with kinetic modeling, was significantly smaller than previous models. However, despite its simplicity, it captured key features of ATRA induced differentiation of HL-60 cells. We identified an ensemble of effective model parameters using measurements taken from ATRA-induced HL-60 cells. Using these parameters, model analysis predicted that MAPK activation was bistable as a function of ATRA exposure. Conformational experiments supported ATRA-induced bistability. These findings, combined with other literature evidence, suggest that positive feedback is central to a diversity of cell fate programs.

1 Introduction

2 Understanding the architecture of differentiation programs is an important therapeutic
3 challenge. Differentiation induction chemotherapy (DIC), using agents such as the vita-
4 min A derivative all-trans retinoic acid (ATRA), is a promising approach for the treatment
5 of many cancers (1–3). For example, ATRA treatment induces remission in 80–90% of
6 promyelocytic leukemia (APL) PML-RAR α -positive patients (4), thereby transforming a
7 fatal diagnosis into a manageable disease. However, remission is sometimes not durable
8 and relapsed cases exhibit emergent ATRA resistance (5, 6). To understand the basis of
9 this resistance, we must first understand the ATRA-induced differentiation program. To-
10 ward this challenge, lessons learned in model systems, such as the lineage-uncommitted
11 human myeloblastic cell line HL-60, could inform our analysis of the more complex dif-
12 ferentiation programs occurring in patients. Patient derived HL-60 leukemia cells have
13 been a durable experimental model since the 1970's to study differentiation (7). HL-60
14 undergoes cell cycle arrest and either myeloid or monocytic differentiation following stim-
15 ulation; ATRA induces G1/G0-arrest and myeloid differentiation in HL-60 cells, while 1,25-
16 dihydroxy vitamin D3 (D3) induces arrest and monocytic differentiation. Commitment to
17 cell cycle arrest and differentiation requires approximately 48 hr of treatment, during which
18 HL-60 cells undergo two division cycles.

19 Sustained mitogen-activated protein kinase (MAPK) activation is a defining feature of
20 ATRA-induced HL-60 differentiation. ATRA drives sustained MEK-dependent activation
21 of the Raf/MEK/ERK pathway, leading to arrest and differentiation (8). MEK inhibition re-
22 sults in the loss of ERK and Raf phosphorylation, and the failure to arrest and differentiate
23 (9). ATRA (and its metabolites) are ligands for the hormone activated nuclear transcrip-
24 tion factors retinoic acid receptor (RAR) and retinoid X receptor (RXR) (10). RAR/RXR
25 activation is necessary for ATRA-induced Raf phosphorylation (9), and the formation of
26 an ATRA-inducible signalsome complex at the membrane which drives MAPK activation

27 through a yet to be identified kinase activity. While the makeup of the signalsome com-
28 plex is not yet known, we do know that it is composed of Src family kinases Fgr and Lyn,
29 PI3K, c-Cbl, Slp76, and KSR, as well as IRF-1 transcription factors (11–15). Signalsome
30 formation and activity is driven by ATRA-induced expression of CD38 and the putative
31 heterotrimeric Gq protein-coupled receptor BLR1 (16, 17). BLR1, identified as an early
32 ATRA (or D3)-inducible gene using differential display (18), is necessary for MAPK ac-
33 tivation and differentiation (17), and is also involved with signalsome activity. Studies
34 of the BLR1 promoter identified a 5' 17bp GT box approximately 1 kb upstream of the
35 transcriptional start that conferred ATRA responsiveness (17). Members of the BLR1
36 transcriptional activator complex, e.g. NFATc3 and CREB, are phosphorylated by ERK,
37 JNK or p38 MAPK family members suggesting positive feedback between the signalsome
38 and MAPK activation (19). BLR1 overexpression enhanced Raf phosphorylation and ac-
39 celerated terminal differentiation, while Raf inhibition reduced BLR1 expression and dif-
40 ferentiation (20). BLR1 knock-out cells failed to activate Raf or differentiate in the pres-
41 ence of ATRA (20). Interestingly, both the knockdown or inhibition of Raf, also reduced
42 BLR1 expression and functional differentiation (20). Thus, the expression of signalsome
43 components e.g., BLR1 was Raf dependent, while Raf activation depended upon the sig-
44 nalsome. A recent computational study of ATRA-induced differentiation in HL-60 cells
45 suggested that the BLR1-MAPK positive feedback circuit was sufficient to explain ATRA-
46 induced sustained MAPK activation, and the expression of a limited number of functional
47 differentiation markers (21). Model analysis also suggested that Raf was the most distinct
48 of the MAPK proteins. However, this previous study developed and analyzed a complex
49 model, thus leaving open the critical question of what is the minimal positive feedback
50 circuit required to drive ATRA-induced differentiation.

51 In this study, we explored this question using a minimal mathematical model of the
52 key architectural feature of ATRA induced differentiation of HL-60 cells, namely positive

53 feedback between an ATRA-inducible signalsome complex and MAPK activation. The
54 ATRA responsive signalsome-MAPK circuit was then used to drive a downstream gene
55 expression program which encoded for the expression of functional differentiation mark-
56 ers. The effective model used a novel framework which integrated logical rules with ki-
57 netic modeling to describe gene expression and protein regulation, while largely relying
58 upon biophysical parameters from the literature. This formulation significantly reduced
59 the size and complexity of the model compared to the previous study of Tasseff et al.,
60 while increasing the breadth of the biology described (21). The effective model, despite
61 its simplicity, captured key features of ATRA induced differentiation of HL-60 cells. Model
62 analysis predicted the bistability of MAPK activation as a function of ATRA exposure; con-
63 formational experiments supported ATRA-induced bistability. Model simulations were also
64 consistent with measurements of the influence of MAPK inhibitors, and the failure of BLR1
65 knockout cells to differentiate when exposed to ATRA. Lastly, we showed by through im-
66 munoprecipitation studies, that the guanine nucleotide exchange factor Vav1 is potentially
67 a new ATRA-inducible member of the signalsome complex. Taken together, these findings
68 when combined with other literature evidence, suggested that positive feedback architec-
69 tures are central to differentiation programs generally, and necessary for ATRA-induced
70 differentiation.

71 **Results**

72 We constructed an effective model of ATRA-induced HL-60 differentiation which described
73 signaling and gene expression events following the addition of ATRA (Fig. 1). The model
74 connectivity was developed from literature and the studies presented here (Table 1). We
75 decomposed the ATRA program into three modules; a signal initiation module that sensed
76 and transformed the ATRA signal into activated cRaf-pS621 and the ATRA-RXR/RAR
77 (Trigger) signals (Fig. 1A); a signal integration module that controlled the expression of
78 upstream transcription factors given cRaf-pS621 and activated Trigger signals (Fig. 1B);
79 and a phenotype module which encoded the expression of functional differentiation mark-
80 ers from the ATRA-inducible transcription factors (Fig. 1C). Each component of these
81 modules was described by a mRNA and protein balance equation. Additionally, the sig-
82 nal initiation module also described the abundance of activated species e.g., Trigger and
83 cRaf-pS621 whose values were derived from unactivated Trigger and cRaf protein levels.
84 Lastly, because the population of HL-60 cells was dividing (at least before ATRA-induced
85 cell cycle arrest), we also considered a dilution term in all balance equations. The sig-
86 nal initiation module contained nine differential equations, while the signal integration and
87 phenotype modules were collectively encoded by 54 differential equations. Model param-
88 eters were taken literature (Table 2), or estimated from experimental data using heuristic
89 optimization (see materials and methods).

90 The signal initiation module recapitulated sustained signalsome and MAPK activation
91 following exposure to $1\mu\text{M}$ ATRA (Fig. 2A-B). An ensemble of effective model param-
92 eters was estimated by minimizing the difference between simulations and time-series
93 measurements of BLR1 mRNA and cRaf-pS621 following the addition of $1\mu\text{M}$ ATRA. We
94 focused on the S621 phosphorylation site of cRaf since enhanced phosphorylation at
95 this site is a defining characteristic of sustained MAPK activation in HL-60. The effective
96 model captured both ATRA-induced BLR1 expression (Fig. 2A) and sustained phospho-

97 phosphorylation of cRaf-pS621 (Fig. 2B) in a growing population of HL-60 cells. Together, the
98 reinforcing positive feedback between the signalsome and MAPK led to sustained activation
99 over multiple cellular generations. However, the effective model failed to capture the
100 decline of BLR1 message after 48 hr of ATRA exposure. This suggested that we captured
101 the logic leading to the onset of differentiation, but failed to describe program shutdown.
102 Next, we tested the response of the signal initiation module to different ATRA dosages.

103 The signal initiation model was bistable with respect to ATRA induction (Fig. 2C-D).
104 Phaseplane analysis predicted two stable steady-states when ATRA was present below
105 a critical threshold, and only a single steady-state above the threshold (Fig. 2C). In the
106 lower stable state, neither the signalsome nor cRaf-pS621 were present (thus, the differ-
107 entiation program was deactivated). However, at the high stable state, both the signal-
108 some and cRaf-pS621 were present, allowing for sustained activation and differentiation.
109 Interestingly, when ATRA was above a critical threshold, only the activated state was ac-
110 cessible (Fig. 2D). To test these findings, we first identified the ATRA threshold. We
111 exposed HL-60 cells to different ATRA concentrations for 72 hr (Fig. 2E). Morphological
112 changes associated with differentiation were visible for ATRA \geq 0.25 μ M, suggesting the
113 critical ATRA threshold was near this concentration. Next, we conducted ATRA washout
114 experiments to determine if activated cells remained activated in the absence of ATRA.
115 HL-60 cells locked into an activated state remained activated following ATRA withdraw-
116 (Fig. 3). This sustained activation resulted from reinforcing feedback between the sig-
117 nalsome and the MAPK pathway. Thus, following activation, if we inhibited or removed
118 elements from the signal initiation module we expected the signalsome and MAPK signals
119 to decay. We simulated ATRA induced activation in the presence of kinase inhibitors, and
120 without key circuit elements. Consistent with experimental results using multiple MAPK
121 inhibitors, ATRA activation in the presence of MAPK inhibitors lowered the steady-state
122 value of signalsome (Fig. 3A). In the presence of BLR1, the signalsome and cRaf-pS621

signals were maintained following ATRA withdraw (Fig. 3B, gray). On the other hand, BLR1 deletion removed the ability of the circuit to maintain a sustained MAPK response following the withdraw of ATRA (Fig. 3B, blue). Lastly, washout experiments in which cells were exposed to $1\mu\text{M}$ ATRA for 24 hr, and then transferred to fresh media without ATRA, confirmed the persistence of the self sustaining activated state for up to 144 hr (Fig. 3C). Thus, these experiments confirmed that reinforcing positive feedback likely drives the ATRA-induced differentiation program. Next, we analyzed the ATRA-induced downstream gene expression program following signalsome and cRaf activation.

The signal integration and phenotype modules described ATRA-induced gene expression in wild-type HL-60 cells (Fig. 4). The signal initiation module produced two outputs, activated Trigger and cRaf-pS621 which drove the expression of ATRA-induced transcription factors, which then in turn activated the phenotypic program. In particular, Trigger (a surrogate for the RAR α /RXR transcriptional complex) regulated the expression of the transcription factors CCATT/enhancer binding protein α (C/EBP α), PU.1, and EGR1. In turn, these transcription factors, in combination with cRaf-pS621, regulated the expression of downstream phenotypic markers such as CD38, CD11b or P47Phox. We assembled the connectivity of the signal integration and phenotypic programs driven by Trigger and cRaf-pS621 from literature (Table 1). We estimated the parameters for the signal initiation, and phenotype modules from steady-state and dynamic measurements of transcription factor and phenotypic marker expression following the addition of ATRA (22–25). However, the bulk of the model parameters were taken from directly from literature (26) and were not estimated in this study (see materials and methods). The model simulations captured the time dependent expression of CD38 and CD11b following the addition ATRA (Fig. 4A), and the steady-state for signal integration and phenotypic markers (Fig. 4B). Lastly, we used the *predicted* values of the p21 and E2F protein abundance to estimate a black-box model of ATRA-induced G0 arrest (Fig. 5). The phenotype module predicted p21

149 expression significantly increased and E2F expression decreased, in response to ATRA
150 exposure (Fig. 5A). We then used the ratio of these values in a polynomial model to cal-
151 culate the fraction of HL-60 cells in G0 arrest following the addition of ATRA (Fig. 5B). The
152 third-order polynomial model captured the trend in measured G0-arrest values as a func-
153 tion of time, and was robust to uncertainty in the measured data (Fig. 5B, gray). Taken
154 together, the output of the signal integration and phenotypic modules was consistent with
155 time-series and steady-state measurements, thereby validating the assumed molecular
156 connectivity. Moreover, outputs from the phenotype module described the trend in ATRA-
157 induced G0 cell cycle arrest. Next, we explored which nodes and interactions between
158 nodes in the signal integration module most influenced the system response.

159 The PU.1 and AP1 proteins were important regulators of ATRA-induced signal inte-
160 gration and phenotypic change (Fig. 6). We conducted pairwise knockout simulations of
161 genes in the signal integration and phenotype modules to estimate which nodes controlled
162 the processing of the Trigger and cRaF-S621 signals. The difference between the sys-
163 tem state with and without the gene knockouts (encoded as a state displacement matrix)
164 was decomposed using Singular Value Decomposition (SVD). A panel of twenty param-
165 eter sets was sampled, and the average displacement matrix was decomposed. The
166 first four modes described >99% of the gene knockout variance, with the most important
167 components of these modes being the PU.1 and AP1 proteins, and to a much lesser ex-
168 tent Gfi1 and C/EBPa (Fig. 6A). To better understand which connections involving the
169 PU.1 and AP1 proteins were important, we simulated the pairwise deletion of interac-
170 tions between these proteins and their respective regulatory targets. SVD decomposition
171 of the state displacement matrix assembled from the pairwise deletion of interactions,
172 suggested the first five modes accounted for >99% of the variance resulting from dele-
173 tion of the interactions. The most sensitive interactions for the PU.1 protein involved the
174 C/EBPa-dependent regulation of P47Phox expression, and to a lesser extent AP1 and

¹⁷⁵ EGR1 expression (Fig. 6B). On the other other, the most sensitive connections for AP1
¹⁷⁶ involved the C/EBPa-dependent regulation of p21 expression, and the mutual activation
¹⁷⁷ of PU.1 and AP1 expression. Taken together, these results suggested that the PU.1 and
¹⁷⁸ AP1 proteins acted as important self-reinforcing regulators for both the signal integration
¹⁷⁹ and phenotype modules. The analysis suggested that the PU.1 signaling axis promoted
¹⁸⁰ the formation of the neutrophil NADPH oxidase (through p47Phox), while AP1 was re-
¹⁸¹ sponsible for cell cycle arrest (through p21). However, this analysis did not give insight
¹⁸² into which upstream components of the signal initiation module were important. Toward
¹⁸³ this question, we explored the composition and regulation of the signalsome complex by
¹⁸⁴ experimentally interrogating a panel of possible Raf interaction partners.

¹⁸⁵ The composition of the signalsome, and the kinase ultimately responsible for medi-
¹⁸⁶ ating ATRA-induced Raf activation is currently unknown. To explore this question, we
¹⁸⁷ conducted immunoprecipitation and subsequent Western blotting to identify physical in-
¹⁸⁸ teractions between Raf and 19 putative interaction partners. A panel of 19 possible Raf
¹⁸⁹ interaction partners (kinases, GTPases, scaffolding proteins etc) was constructed based
¹⁹⁰ upon known signaling pathways. We did not consider the most likely binding partner, the
¹⁹¹ small GTPase RAS, as previous studies have ruled it out in MAPK activation in HL-60 cells
¹⁹² (20, 27). Total Raf was used as a bait protein for the immunoprecipitation studies. Interro-
¹⁹³ gation of the Raf interactome suggested Vav1 was involved with ATRA-induced initiation
¹⁹⁴ of MAPK activity (Fig. 7). Western blot analysis using total Raf and pS621 Raf specific
¹⁹⁵ antibodies confirmed the presence of the bait protein, total and phosphorylated forms, in
¹⁹⁶ the immunoprecipitate (Fig. 7A). Of the 19 proteins sampled, Vav1, Src, CK2, Akt, and
¹⁹⁷ 14-3-3 precipitated with Raf, suggesting a direct physical interaction was possible. How-
¹⁹⁸ ever, only the associations between Raf and Vav1 and Raf and Src were ATRA-inducible
¹⁹⁹ (Fig. 7). Furthermore, the Vav1 and Src associations were correlated with pS621 Raf
²⁰⁰ abundance in the precipitate. Others proteins e.g., CK2, Akt and 14-3-3, generally bound

201 Raf regardless of phosphorylation status or ATRA treatment. The remaining 14 proteins
202 were expressed in whole cell lysate (Fig. 7B), but were not detectable in the precipitate
203 of Raf IP. Treatment with the Raf kinase inhibitor GW5074 following ATRA exposure re-
204 duced the association of both Vav1 with Raf and Src with Raf (Fig. 7), although the signal
205 intensity for Src was notably weak. However, GW5074 did not influence the association
206 of CK2 or 14-3-3 with Raf, further demonstrating their independence from Raf phospho-
207 rylation. Interestingly, the Raf-Akt interaction qualitatively increased following treatment
208 with GW5074; however, it remained unaffected by treatment with ATRA. Src family ki-
209 nases are known to be important in myeloid differentiation (28) and their role in HL-60
210 differentiation has been investigated elsewhere (11). Given the existing work and variable
211 reproducibility in the context of the Raf immunoprecipitate, we did not investigate the role
212 of Src further in this study. Taken together, the immunoprecipitation and GW5074 results
213 implicated Vav1 association to be correlated with Raf activation following ATRA-treatment.
214 Previous studies demonstrated that a Vav1-Slp76-Cbl-CD38 complex plays an important
215 role in ATRA-induced MAPK activation and differentiation of HL-60 cells (13). Here we
216 did not observe direct interaction of Raf with Cbl or Slp76; however, this complex could
217 be involved upstream. Next, we considered the effect of the Raf kinase inhibitor GW5074
218 on functional markers of ATRA-induced growth arrest and differentiation.

219 Inhibition of Raf kinase activity modulated MAPK activation and differentiation mark-
220 ers following ATRA exposure (Fig. 7D-F). ATRA treatment alone statistically significantly
221 increased the G1/G0 percentage over the untreated control, while GW5074 alone had a
222 negligible effect on the cell cycle distribution (Fig. 7D). Surprisingly, the combination of
223 GW5074 and ATRA statistically significantly increased the G1/G0 population ($82 \pm 1\%$)
224 compared with ATRA alone ($61 \pm 0.5\%$). Increased G1/G0 arrest following the combined
225 treatment with GW5074 and ATRA was unexpected, as the combination of ATRA and the
226 MEK inhibitor (PD98059) has been shown previously to decrease ATRA-induced growth

227 arrest (8). However, growth arrest is not the sole indication of functional differentiation.
228 Expression of the cell surface marker CD11b has also been shown to coincide with HL-60
229 cells myeloid differentiation (29). We measured CD11b expression, for the various treat-
230 ment groups, using immuno-fluorescence flow cytometry 48 hr post-treatment. As with
231 G1/G0 arrest, ATRA alone increased CD11b expression over the untreated control, while
232 GW5074 further enhanced ATRA-induced CD11b expression (Fig. 7E). GW5074 alone
233 had no statistically significant effect on CD11b expression, compared with the untreated
234 control. Lastly, the inducible reactive oxygen species (ROS) response was used as a func-
235 tional marker of differentiated neutrophils (16). We measured the ROS response induced
236 by the phorbol ester 12-O-tetradecanoylphorbol-13-acetate (TPA) using flow cytometry.
237 Untreated cells showed no discernible TPA response, with only $7.0 \pm 3.0\%$ ROS induction
238 (Fig. 7F). Cells treated with ATRA had a significantly increased TPA response, $53 \pm 7\%$
239 ROS induction 48 hr post-treatment. Treatment with both ATRA and GW5074 statistically
240 significantly reduced ROS induction ($22 \pm 0.6\%$) compared to ATRA alone. Interestingly,
241 Western blot analysis did not detect a GW5074 effect on ATRA-induced expression of
242 p47phox, a required upstream component of the ROS response (Fig. 7F, bottom). Thus,
243 the inhibitory effect of GW5074 on inducible ROS might occur downstream of p47phox
244 expression. However, the ROS producing complex is MAPK dependent, therefore it is
245 also possible that GW5074 inhibited ROS production by interfering with MAPK activation
246 (in which case the p47Phox marker might not accurately reflect phenotypic conversion
247 and differentiation).

248 **Discussion**

249 In this study, we presented an effective model of ATRA-inducible differentiation of HL-60
250 cells. The model consisted of three modules: a signal initiation module that sensed and
251 transformed the ATRA signal into activated cRaf-pS621 and the ATRA-RXR/RAR (Trig-
252 ger) signals; a signal integration module that controlled the expression of upstream tran-
253 scription factors given cRaf-pS621 and activated Trigger signals; and a phenotype mod-
254 ule which encoded the expression of functional differentiation markers from the ATRA-
255 inducible transcription factors. The model described the transcription and translation of
256 genes in each module, and signaling events in each module in a growing population of
257 HL-60 cells. Model parameters were largely taken from literature, however, unknown
258 coefficients were estimated from protein measurements in HL-60 cells following ATRA
259 exposure. Despite its simplicity, the effective model captured key features of the ATRA
260 induced differentiation such as sustained MAPK activation, and bistability with respect
261 to ATRA exposure. The model also described the expression of upstream transcription
262 factors which regulated the expression of differentiation markers. Lastly, analysis of the
263 response of the model to perturbations identified PU.1 and AP1 as master regulators of
264 ATRA-induced differentiation. We also reported a new ATRA-inducible component of the
265 signalsome, Vav1. Vav1 is a guanine nucleotide exchange factor for Rho family GTPases
266 that activate pathways leading to actin cytoskeletal rearrangements and transcriptional al-
267 terations (30). The Vav1/Raf association correlated with Raf activity, was ATRA-inducible
268 and decreased after treatment with the Raf inhibitor GW5074.

269 Naturally occurring cell fate decisions often incorporate reinforcing feedback and bista-
270 bility (31, 32). One of the most well studied cell fate circuits is the Mos mitogen-activated
271 protein kinase cascade in *Xenopus* oocytes. This cascade is activated when oocytes are
272 induced by the steroid hormone progesterone (33). The MEK-dependent activation of
273 p42 MAPK stimulates the accumulation of the Mos oncprotein, which in turn activates

274 MEK, thereby closing the feedback loop. This is similar to the signal initiation module
275 presented here; ATRA drives signalsome formation, which activates MAPK, which in turn
276 leads to more signalsome activation. Thus, while HL-60 and *Xenopus* oocytes are vastly
277 different biological models, their cell fate programs share a similar architectural feature.
278 Reinforcing feedback and bistability has also been implicated in hematopoietic cell fate
279 determination. Laslo et al showed that the counter antagonistic repressors, Gfi-1 and
280 Egr-1/2 (whose expression is tuned by PU.1 and C/EBPa), encodes a bistable switch that
281 results in a macrophage, neutrophil or a mixed lineage population depending upon PU.1
282 and C/EBPa expression (32). The current model contained the Gfi-1 and Egr-1/2 agonis-
283 tic switch; however, its significance was unclear for HL-60 cells. The expression of Gfi-1,
284 Egr-1/2, C/EBPa and PU.1 was not consistent with the canonical lineage pattern expected
285 from literature. For example, Egr-1/2 expression (associated with a macrophage lineage)
286 increased, while Gfi-1 expression (associated with a neutrophil lineage) remained con-
287 stant following ATRA exposure. Literature evidence in nonmalignant myelomonocytic fate
288 selection has shown that Gfi-1 and EGR-1/2 promote granulocytic and monocytic differ-
289 entiation, respectively (32). Thus, HL-60 cells, which are a less mature cancer cell line,
290 exhibited a non-canonical expression pattern. Other unrelated cell fate decisions such
291 as programmed cell death have also been suggested to be bistable (34). Still more bio-
292 chemical networks important to human health, for example the human coagulation or
293 complement cascades, also feature strong positive feedback elements (35). Thus, while
294 reinforcing feedback is often undesirable in human engineered systems, it is at the core
295 of a diverse variety of cell fate programs and other networks important to human health.

296 Analysis of the signal integration and phenotype modules suggested that PU.1 and
297 AP1 regulated distinct phenotypic axes following ATRA exposure. PU.1, a member of
298 the ets transcription factor family, is a well known regulatory protein in granulocyte and
299 monocyte development (36). The relative level of PU.1 and C/EBPa is thought to regulate

300 macrophage versus neutrophil cell fate decisions in granulocytic macrophage progenitor cells (37). However, in previous studies we showed that PU.1 has additional non-
301 canonical function as it is highly expressed following the addition of ATRA to HL-60 cells.
302 Analysis of the model in this study suggested that the C/EBPa dependent interaction of
303 PU.1 with the *NCF1* gene, which encodes for the P47Phox protein, was the most sen-
304 sitive PU.1 connection. P47Phox, also known as neutrophil cytosol factor 1, is one of
305 four cytosolic subunits of the multi-protein NADPH oxidase complex found in neutrophils
306 (38). This enzyme is responsible for reactive oxygen species (ROS) production, a key
307 component of the anti-microbial function of neutrophils. PU.1 also acted in concert with
308 the activator protein 1 (AP-1) transcription factor to regulate p21 expression, a second
309 phenotypic outcome of ATRA-induced differentiation. The AP-1 transcription factor reg-
310 ulates gene expression in response to a variety of stimuli. However, in the context of
311 ATRA-induced differentiation, AP1 have been shown to
312

313 Immunoprecipitation studies identified a limited number of ATRA-dependent and -
314 independent Raf interaction partners. While we were unable to detect the association
315 of Raf with common kinases and GTPases such as PKC, PKA, p38, Rac and Rho, we
316 did establish potential interactions between Raf and key partners such as Vav1, Src, Akt,
317 CK2 and 14-3-3. All of these partners are known to be associated with Raf activation
318 or function. Src is known to bind Raf through an SH2 domain, and this association has
319 been shown to be dependent of the serine phosphorylation of Raf (39). Thus, an ATRA in-
320 ductible Src/Raf association may be a result of ATRA-induced Raf phosphorylation at S259
321 or S621. We also identified an interaction between Raf and the Ser/Thr kinases Akt and
322 CK2. Akt can phosphorylate Raf at S259, as demonstrated by studies in a human breast
323 cancer line (40). CK2 can also phosphorylate Raf, although the literature has traditionally
324 focused on S338 and not S621 or S259(41). However, neither of these kinase interactions
325 were ATRA-inducible, suggesting their association with Raf alone was not associated with

326 ATRA-induced Raf phosphorylation. The adapter protein 14-3-3 was also constitutively
327 associated with Raf. The interaction between Raf and 14-3-3 has been associated with
328 both S621 and S259 phosphorylation and activity (42). Additionally, the association of
329 Raf with 14-3-3 not only stabilized S621 phosphorylation, but also reversed the S621
330 phosphorylation from inhibitory to activating (43). Finally, we found that Vav1/Raf associ-
331 ation correlated with Raf activity, was ATRA-inducible and decreased after treatment with
332 GW5074. The presence of Vav1 in Raf/Grb2 complexes has been shown to correlate with
333 increased Raf activity in mast cells (44). Furthermore, studies on Vav1 knockout mice
334 demonstrated that the loss of Vav1 resulted in deficiencies of ERK signaling for both T-
335 cells as well as neutrophils (45, 46). Interestingly, while an integrin ligand-induced ROS
336 response was blocked in Vav1 knockout neutrophils, TPA was able to bypass the Vav1
337 requirement and stimulate both ERK phosphorylation and ROS induction (46). In this
338 study, the TPA-induced ROS response was dependent upon Raf kinase activity, and was
339 mitigated by the addition of GW5074. It is possible that Vav1 is downstream of various
340 integrin receptors but upstream of Raf in terms of inducible ROS responses. Vav1 has
341 also been shown to associate with a Cbl-Slp76-CD38 complex in an ATRA-dependent
342 manner; furthermore, transfection of HL-60 cells with Cbl mutants that fail to bind CD38,
343 yet still bind Slp76 and Vav1, prevents ATRA-induced MAPK activation (13). The literature
344 suggest a variety of possible receptor-signaling pathways, which involve Vav1, for MAPK
345 activation; moreover, given the ATRA-inducible association Vav1 may play a direct role in
346 Raf activation.

347 We hypothesized that Vav1 is a member of an ATRA-inducible complex which propels
348 sustained MAPK activation, arrest and differentiation. Initially, ATRA-induced Vav1 ex-
349 pression drives increased association between Vav1 and Raf. This increased interaction
350 facilitates phosphorylation and activation of Raf by pre-bound Akt and/or CK2 at S621
351 or perhaps S259. Constitutively bound 14-3-3 may also stabilize the S621 phosphory-

352 lation, modulate the activity and/or up-regulate autophosphorylation. Activated Raf can
353 then drive ERK activation, which in turn closes the positive feedback loop by activating
354 Raf transcription factors e.g., Sp1 and/or STAT1 (47–50). We tested this working hy-
355 pothesis using mathematical modeling. The model recapitulated both ATRA time-course
356 data as well as the GW5074 inhibitor effects. This suggested the proposed Raf-Vav1
357 architecture was at least consistent with the experimental studies. Further, analysis of
358 the Raf-Vav1 model identified bistability in ppERK levels. Thus, two possible MAPK ac-
359 tivation branches were possible for experimentally testable ATRA values. The analysis
360 also suggested the ATRA-induced Raf-Vav1 architecture could be locked into a sustained
361 signaling mode (high ppERK) even in the absence of a ATRA signal. This locked-in prop-
362 erty could give rise to an ATRA-induction memory. We validated the treatment memory
363 property predicted by the Raf-Vav1 circuit experimentally using ATRA-washout experi-
364 ments. ERK phosphorylation levels remained high for more then 96 hr after ATRA was
365 removed. Previous studies demonstrated that HL-60 cells possessed an inheritable mem-
366 ory of ATRA stimulus (51). Although the active state was self-sustaining, the inactive state
367 demonstrated considerable robustness to perturbation. For example, we found that 50x
368 overexpression of Raf was required to reliably lock MAPK into the activated state, while
369 small perturbations had almost no effect on ppERK levels over the entire ensemble. CD38
370 expression correlated with the ppERK, suggesting its involvement in the signaling com-
371 plex. Our computational and experimental results showed that positive feedback, through
372 ERK-dependent Raf expression, could sustain MAPK signaling through many division cy-
373 cles. Such molecular mechanisms could underly aspects of cellular memory associated
374 to consecutive ATRA treatments.

375 There were several issues that can be explored further with the effective ATRA differ-
376 entiation model. First, there was likely missing connectivity in the effective differentiation
377 circuit. Decreasing BLR1 expression with simultaneously sustained cRaf-pS261 activa-

378 tion was not captured by the current network architecture. This suggested that signal-
379 some, once activated, had a long lifetime as decreased BLR1 expression did not impact
380 cRaf-pS261 abundance. We could model this by separating signalsome formation into an
381 inactive precursor pool that is transformed to a long-lived activated signalsome by MAPK
382 activation. We should also explore adding additional downstream biological modules to
383 this skeleton model, for example the upregulation of reactive oxygen markers such as
384 p47Phox or cell cycle arrest components to capture the switch from an actively prolifer-
385 ating population to a population in G0-arrest. Next, the choice of max/min integration
386 rules or the particular form of the transfer functions could also be explored. Integration
387 rules other than max/min could be used, such as the mean or the product, assuming the
388 range of the transfer functions is always $f \in [0, 1]$. Alternative integration rules might
389 have different properties which could influence model identification or performance. For
390 example, a mean integration rule would be differentiable, allowing derivative-based opti-
391 mization approaches to be used. The form of the transfer function could also be explored.
392 We choose hill-like functions because of their prominence in the systems and synthetic
393 biology community. However, many other transfer functions are possible.

394 **Materials and Methods**

395 *Effective gene expression model equations.* We decomposed the ATRA-induced differ-
 396 entiation program into three modules; a signal initiation module that sensed and trans-
 397 formed the ATRA signal into activated cRaf-pS621 and the ATRA-RXR/RAR (activated
 398 Trigger) signals; a signal integration module that controlled the expression of upstream
 399 transcription factors given cRaf-pS621 and activated Trigger signals; and a phenotype
 400 module which encoded the expression of functional differentiation markers from the ATRA-
 401 inducible transcription factors. The output of the signal initiation module was the input to
 402 the gene expression model. For each gene $j = 1, 2, \dots, \mathcal{G}$, we modeled both the mRNA
 403 (m_j), protein (p_j) and signaling species abundance:

$$\frac{dm_j}{dt} = r_{T,j} - (\mu + \theta_{m,j}) m_j + \lambda_j \quad (1)$$

$$\frac{dp_j}{dt} = r_{X,j} - (\mu + \theta_{p,j}) p_j \quad (2)$$

$$g(p_1, \dots, p_{\mathcal{G}}, \kappa) = 0 \quad (3)$$

404 The terms $r_{T,j}$ and $r_{X,j}$ denote the specific rates of transcription, and translation while
 405 the terms $\theta_{m,j}$ and $\theta_{p,j}$ denote first-order degradation constants for mRNA and protein,
 406 respectively. The specific transcription rate $r_{T,j}$ was modeled as the product of a kinetic
 407 term $\bar{r}_{T,j}$ and a control term u_j which described how the abundance of transcription fac-
 408 tors, or other regulators influenced the expression of gene j . The kinetic transcription
 409 term $\bar{r}_{T,j}$ was modeled as:

$$\bar{r}_{T,j} = V_T^{max} \left(\frac{L_{T,o}}{L_{T,j}} \right) \left(\frac{G_j}{K_T + G_j} \right) \quad (4)$$

410 where the maximum gene expression rate V_T^{max} was defined as the product of a char-
 411 acteristic transcription rate constant (k_T) and the abundance of RNA polymerase (R_1),

412 $V_T^{max} = k_T(R_1)$. The $(L_{T,o}/L_{T,j})$ term denotes the ratio of transcription read lengths; $L_{T,o}$
 413 represents a characteristic gene length, while $L_{T,j}$ denotes the length of gene j . Thus,
 414 the ratio $(L_{T,o}/L_{T,j})$ is a gene specific correction to the characteristic transcription rate
 415 V_T^{max} . The degradation rate constants were defined as $\theta_{m,j}$ and $\theta_{p,j}$ denote characteristic
 416 degradation constants for mRNA and protein, respectively. Lastly, the λ_j term denotes the
 417 constitutive rate of expression of gene j .

418 The gene expression control term $0 \leq u_j \leq 1$ depended upon the combination of fac-
 419 tors which influenced the expression of gene j . If the expression of gene j was influenced
 420 by $1, \dots, m$ factors, we modeled this relationship as $u_j = \mathcal{I}_j(f_{1j}(\cdot), \dots, f_{mj}(\cdot))$ where
 421 $0 \leq f_{ij}(\cdot) \leq 1$ denotes a regulatory transfer function quantifying the influence of factor i
 422 on the expression of gene j , and $\mathcal{I}_j(\cdot)$ denotes an integration rule which combines the
 423 individual regulatory inputs for gene j into a single control term. In this study, the integra-
 424 tion rule governing gene expression was the weighted fraction of promoter configurations
 425 that resulted in gene expression (52):

$$u_j = \frac{W_{R_{1,j}} + \sum_n W_{nj} f_{nj}}{1 + W_{R_{1,j}} + \sum_d W_{dj} f_{dj}} \quad (5)$$

426 The numerator, the weighted sum (with weights W_{nj}) of promoter configurations leading to
 427 gene expression, was normalized by all possible promoter configurations. The likelihood
 428 of each configuration was quantified by the transfer function f_{nj} (which we modeled using
 429 hill like functions), while the lead term in the numerator $W_{R_{1,j}}$ denotes the weight of con-
 430 stitutive expression for gene j . Given this formulation, the rate of constitutive expression
 431 was then given by:

$$\lambda_j = \bar{r}_{T,j} \left(\frac{W_{R_{1,j}}}{1 + W_{R_{1,j}}} \right) \quad (6)$$

432 If a gene expression process had no modifying factors, $u_j = 1$. Lastly, the specific trans-

433 lation rate was modeled as:

$$r_{X,j} = V_X^{\max} \left(\frac{L_{X,o}}{L_{X,j}} \right) \left(\frac{m_j}{K_X + m_j} \right) \quad (7)$$

434 where V_X^{\max} denotes a characteristic maximum translation rate estimated from literature,
435 and K_X denotes a translation saturation constant. The characteristic maximum translation
436 rate was defined as the product of a characteristic translation rate constant (k_X) and
437 the Ribosome abundance (R_2), $V_X^{\max} = k_X (R_2)$. As was the case for transcription, we
438 corrected the characteristic translation rate by the ratio of the length of a characteristic
439 transcription normalized by the length of transcript j .

440 *Signaling model equations.* The signal initiation, and integration modules required the
441 abundance of cRaf-pS621 and ATRA-RXR/RAR (activated Trigger) as inputs. However,
442 our base model described only the abundance of inactive proteins e.g., cRaf or RXR/RAR
443 but not the activated forms. To address this issue, we estimated pseudo steady state
444 approximations for the abundance of cRaf-pS621 and activated Trigger (shown generally
445 as Eq (3)). The abundance of activated trigger ($x_{a,1}$) was estimated directly from the
446 RXR/RAR abundance ($x_{u,1}$):

$$x_{a,1} \sim x_{u,1} \left(\frac{\alpha \cdot \text{ATRA}}{1 + \alpha \cdot \text{ATRA}} \right) \quad (8)$$

447 where α denotes a gain parameter; $\alpha = 0.0$ if ATRA is less than a threshold, and $\alpha = 0.1$
448 if ATRA is greater than the differentiation threshold. The abundance of cRaf-pS621 was
449 estimated by making the pseudo steady state approximation on the cRaf-pS621 balance.
450 The abundance of an activated signaling species i was given by:

$$\frac{dx_i}{dt} = r_{+,i}(\mathbf{x}, \mathbf{k}) - (\mu + k_{d,i}) x_i \quad i = 1, \dots, \mathcal{M} \quad (9)$$

451 The quantity x_i denotes concentration of signaling species i , while \mathcal{R} and \mathcal{M} denote
 452 the number of signaling reactions and signaling species in the model, respectively. The
 453 term $r_{+,i}(\mathbf{x}, \mathbf{k})$ denotes the rate of generation of activated species i , while μ denotes
 454 the specific growth rate, and $k_{d,i}$ denotes the rate constant controlling the non-specific
 455 degradation of x_i . We neglected deactivation reactions e.g., phosphatase activities. We
 456 assumed that signaling processes were fast compared to gene expression; this allowed
 457 us to approximate the signaling balance as:

$$x_i^* \simeq \frac{r_{+,i}(\mathbf{x}, \mathbf{k})}{(\mu + k_{d,i})} \quad i = 1, \dots, \mathcal{M} \quad (10)$$

458 The generation rate was written as the product of a kinetic term ($\bar{r}_{+,i}$) and a control term
 459 (v_i). The control terms $0 \leq v_j \leq 1$ depended upon the combination of factors which in-
 460 fluenced rate process j . If rate j was influenced by $1, \dots, m$ factors, we modeled this
 461 relationship as $v_j = \mathcal{I}_j(f_{1j}(\cdot), \dots, f_{mj}(\cdot))$ where $0 \leq f_{ij}(\cdot) \leq 1$ denotes a regulatory
 462 transfer function quantifying the influence of factor i on rate j . The function $\mathcal{I}_j(\cdot)$ is an
 463 integration rule which maps the output of regulatory transfer functions into a control vari-
 464 able. In this study, we used $\mathcal{I}_j \in \{\min, \max\}$ and hill transfer functions (53). If a process
 465 had no modifying factors, $v_j = 1$. The kinetic rate of cRaf-pS621 generation $\bar{r}_{+,cRaf}$ was
 466 modeled as:

$$\bar{r}_{+,cRaf} = k_{+,cRaf} x_s \left(\frac{x_{cRaf}}{K_{+,cRaf} + x_{cRaf}} \right) \quad (11)$$

467 where x_s denotes the signalsome abundance, and $K_{+,cRaf}$ denotes a saturation constant
 468 governing cRaf-pS621 formation. The formation of cRaf-pS621 was regulated by only a
 469 single factor, the abundance of MAPK inhibitor, thus $v_{+,cRaf}$ took the form:

$$v_{+,cRaf} = \left(1 - \frac{I}{K_D + I} \right) \quad (12)$$

470 where I denotes the abundance of the MAPK inhibitor, and K_D denotes the inhibitor
471 affinity.

472 *Estimation of gene expression model parameters.* We estimated parameters appearing
473 in the mRNA and protein balances, the abundance of polymerases and ribosomes, tran-
474 scription and translation rates, the half-life of a typical mRNA and protein, and typical
475 values for the copies per cell of RNA polymerase and ribosomes from literature (Table 2).
476 The saturation constants K_X and K_T were adjusted so that gene expression and trans-
477 lation resulted in gene products on a biologically realistic concentration scale. Lastly, we
478 calculated the concentration for gene G_j by assuming, on average, that a cell had two
479 copies of each gene at any given time. Thus, the bulk of our gene expression model pa-
480 rameters were based directly upon literature values, and were not adjusted during model
481 identification. However, the remaining parameters, e.g., the W_{ij} appearing in the gene
482 expression control laws, or parameters appearing in the transfer functions f_{dij} , were esti-
483 mated from the protein expression and signaling data sets discussed here.

484 Signaling and gene expression model parameters were estimated by minimizing the
485 squared difference between simulations and experimental protein data set j . We mea-
486 sured the squared difference in the scale, fold change and shape for protein j :

$$E_j(\mathbf{k}) = \left(\mathcal{M}_j(t_-) - \hat{y}_j(t_-, \mathbf{k}) \right)^2 + \sum_{i=1}^{\mathcal{T}_j} \left(\hat{\mathcal{M}}_{ij} - \hat{y}_{ij}(\mathbf{k}) \right)^2 + \sum_{i=1}^{\mathcal{T}_j} \left(\mathcal{M}'_{ij} - y'_{ij}(\mathbf{k}) \right)^2 \quad (13)$$

487 The first term in Eqn. (13) quantified the initial *scale* error, directly before the addition
488 of ATRA. In this case, $\mathcal{M}_j(t_-)$ (the approximate concentration of protein j before the
489 addition of ATRA) was estimated from literature. This term was required because the
490 protein measurements were reported as the fold-change; thus, the data was normalized
491 by a control value measured before the addition of ATRA. However, the model operated on
492 a physical scale. The first term allowed the model to capture physically realistic changes

following ATRA addition. The second term quantified the difference in the *fold-change* of protein j as a function of time. The terms $\hat{\mathcal{M}}_{ij}$ and \hat{y}_{ij} denote the scaled experimental observations and simulation outputs (fold-change; protein normalized by control value directly before ATRA addition) at time i from protein j , where T_j denoted the number of time points for data set j . Lastly, the third term of the objective function measured the difference in the *shape* of the measured and simulated protein levels. The scaled value $0 \leq \mathcal{M}'_{ij} \leq 1$ was given by:

$$\hat{\mathcal{M}}_{ij} = \left(\mathcal{M}_{ij} - \min_i \mathcal{M}_{ij} \right) / \left(\max_i \mathcal{M}_{ij} - \min_i \mathcal{M}_{ij} \right) \quad (14)$$

where $\mathcal{M}'_{ij} = 0$ and $\mathcal{M}'_{ij} = 1$ describe the lowest (highest) intensity bands. A similar scaling was used for the simulation output. We minimized the total model residual $\sum_j E_j$ using a heuristic direct-search optimization procedure, subject to box constraints on the parameter values, starting from a random initial parameter guess. Each downhill step was archived and used for ensemble calculations. The optimization procedure (a covariance matrix adaptation evolution strategy) has been reported previously (54).

Estimation of an effective cell cycle arrest model. We formulated an effective N-order polynomial model of the fraction of cells undergoing ATRA-induced cell cycle arrest at time t , $\hat{\mathcal{A}}(t)$, as:

$$\hat{\mathcal{A}}(t) \simeq a_0 + \sum_{i=1}^{N-1} a_i \phi_i(\mathbf{p}(t), t) \quad (15)$$

where a_i were unknown parameters, and $\phi_i(\mathbf{p}(t), t)$ denotes a basis function. The basis functions were dependent upon the system state; in this study, we assumed $N = 4$ and basis functions of the form:

$$\phi_i(\mathbf{p}(t), t) = \left(\frac{t}{T} + \frac{p21}{E2F} \Big|_t \right)^{(i-1)} \quad (16)$$

512 The parameters a_0, \dots, a_3 were estimated directly from cell-cycle measurements (biologi-
513 cal replicates) using least-squares.

514 *Availability of model code.* The signaling and gene expression model equations, and the
515 parameter estimation procedure, were implemented in the Julia programming language.
516 The model equations were solved using the ODE23s routine of the ODE package (55). The
517 model code and parameter ensemble is freely available under an MIT software license
518 and can be downloaded from <http://www.varnerlab.org>.

519 *Cell culture and treatment* Human myeloblastic leukemia cells (HL-60 cells) were grown
520 in a humidified atmosphere of 5% CO₂ at 37°C and maintained in RPMI 1640 from Gibco
521 (Carlsbad, CA) supplemented with 5% heat inactivated fetal bovine serum from Hyclone
522 (Logan, UT) and 1× antibiotic/antimicotic (Gibco, Carlsbad, CA). Cells were cultured in
523 constant exponential growth (56). Experimental cultures were initiated at 0.1×10^6 cells/mL
524 24 hr prior to ATRA treatment; if indicated, cells were also treated with GW5074 (2 μ M) 18
525 hr before ATRA treatment. For the cell culture washout experiments, cells were treated
526 with ATRA for 24 hr, washed 3x with prewarmed serum supplemented culture medium
527 to remove ATRA, and reseeded in ATRA-free media as described. Western blot analysis
528 was performed at incremental time points after removal of ATRA.

529 *Chemicals* All-Trans Retinoic Acid (ATRA) from Sigma-Aldrich (St. Louis, MO) was dis-
530 solved in 100% ethanol with a stock concentration of 5mM, and used at a final concen-
531 tration of 1 μ M (unless otherwise noted). The cRaf inhibitor GW5074 from Sigma-Aldrich
532 (St. Louis, MO) was dissolved in DMSO with a stock concentration of 10mM, and used
533 at a final concentration of 2 μ M. HL-60 cells were treated with 2 μ M GW5074 with or with-
534 out ATRA (1 μ M) at 0 hr. This GW5074 dosage had a negligible effect on the cell cycle
535 distribution, compared to ATRA treatment alone.

536 *Immunoprecipitation and western blotting* Approximately 1.2×10^7 cells were lysed using
537 $400\mu\text{L}$ of M-Per lysis buffer from Thermo Scientific (Waltham, MA). Lysates were cleared
538 by centrifugation at $16,950 \times g$ in a micro-centrifuge for 20 min at 4°C . Lysates were
539 pre-cleared using $100\mu\text{L}$ protein A/G Plus agarose beads from Santa Cruz Biotechnology
540 (Santa Cruz, CA) by inverting overnight at 4°C . Beads were cleared by centrifugation and
541 total protein concentration was determined by a BCA assay (Thermo Scientific, Waltham,
542 MA). Immunoprecipitations were setup by bringing lysate to a concentration of 1g/L in a
543 total volume of $300\mu\text{L}$ (M-Per buffer was used for dilution). The anti-Raf antibody was
544 added at $3\mu\text{L}$. A negative control with no bait protein was also used to exclude the di-
545 rect interaction of proteins with the A/G beads. After 1 hr of inversion at 4°C , $20\mu\text{L}$ of
546 agarose beads was added and samples were left to invert overnight at 4°C . Samples
547 were then washed three times with M-Per buffer by centrifugation. Finally proteins were
548 eluted from agarose beads using a laemmli loading buffer. Eluted proteins were resolved
549 by SDS-PAGE and Western blotting. Total lysate samples were normalized by total protein
550 concentration ($20\mu\text{g}$ per sample) and resolved by SDS-PAGE and Western blotting. Sec-
551 ondary HRP bound antibody was used for visualization. All antibodies were purchased
552 from Cell Signaling (Boston, MA) with the exception of α -p621 Raf which was purchased
553 from Biosource/Invitrogen (Carlsbad, CA), and α -CK2 from BD Biosciences (San Jose,
554 CA).

555 *Morphology assessment* Untreated and ATRA-treated HL-60 cells were collected after
556 72 hr and cytocentrifuged for 3 min at 700 rpm onto glass slides. Slides were air-dried
557 and stained with Wright's stain. Slide images were captured at 40X (Leica DM LB 100T
558 microscope, Leica Microsystems).

559 **Competing interests**

560 The authors declare that they have no competing interests.

561 **Author's contributions**

562 J.V and A.Y directed the study. R.T, H.J, R.B and J.C conducted the cell culture measure-
563 ments. J.V, R.B, W.D, K.R and A.S developed the reduced order HL-60 models and the
564 parameter ensemble. W.D and J.V analyzed the model ensemble, and generated figures
565 for the manuscript. The manuscript was prepared and edited for publication by W.D, A.Y
566 and J.V.

567 **Acknowledgements**

568 We gratefully acknowledge the suggestions from the anonymous reviewers to improve
569 this manuscript.

570 **Funding**

571 We acknowledge the financial support to J.V. by the National Science Foundation CA-
572 REER (CBET-0846876) for the support of R.T. and H.J. In addition, we acknowledge
573 support to A.Y. from the National Institutes of Health (CA 30555, CA152870) and a grant
574 from New York State Stem Cell Science. Lastly, we acknowledge the financial support to
575 J.V. and A.Y. from the National Cancer Institute (#U54 CA143876). The content is solely
576 the responsibility of the authors and does not necessarily represent the official views of
577 the National Cancer Institute or the National Institutes of Health.

578 **References**

- 579 1. Bushue N, Wan YJY (2010) Retinoid pathway and cancer therapeutics. *Adv Drug
580 Deliv Rev* 62: 1285-98.
- 581 2. Tang XH, Gudas LJ (2011) Retinoids, retinoic acid receptors, and cancer. *Annu Rev
582 Pathol* 6: 345-64.
- 583 3. Cheung FSG, Lovicu FJ, Reichardt JKV (2012) Current progress in using vitamin d
584 and its analogs for cancer prevention and treatment. *Expert Rev Anticancer Ther*
585 12: 811-37.
- 586 4. Nilsson B (1984) Probable in vivo induction of differentiation by retinoic acid of
587 promyelocytes in acute promyelocytic leukaemia. *Br J Haematol* 57: 365-71.
- 588 5. Warrell RP Jr (1993) Retinoid resistance in acute promyelocytic leukemia: new
589 mechanisms, strategies, and implications. *Blood* 82: 1949-53.
- 590 6. Freemantle SJ, Spinella MJ, Dmitrovsky E (2003) Retinoids in cancer therapy and
591 chemoprevention: promise meets resistance. *Oncogene* 22: 7305-15.
- 592 7. Breitman TR, Selonick SE, Collins SJ (1980) Induction of differentiation of the hu-
593 man promyelocytic leukemia cell line (HL-60) by retinoic acid. *Proc Natl Acad Sci U
594 S A* 77: 2936–2940.
- 595 8. Yen A, Roberson MS, Varvayanis S, Lee AT (1998) Retinoic acid induced
596 mitogen-activated protein (MAP)/extracellular signal-regulated kinase (ERK) kinase-
597 dependent MAP kinase activation needed to elicit HL-60 cell differentiation and
598 growth arrest. *Cancer Res* 58: 3163–3172.
- 599 9. Hong HY, Varvayanis S, Yen A (2001) Retinoic acid causes MEK-dependent RAF
600 phosphorylation through RARalpha plus RXR activation in HL-60 cells. *Differentia-
601 tion* 68: 55–66.
- 602 10. Mangelsdorf DJ, Ong ES, Dyck JA, Evans RM (1990) Nuclear receptor that identifies
603 a novel retinoic acid response pathway. *Nature* 345: 224–229.

- 604 11. Congleton J, MacDonald R, Yen A (2012) Src inhibitors, PP2 and dasatinib, increase
605 retinoic acid-induced association of Lyn and c-Raf (S259) and enhance MAPK-
606 dependent differentiation of myeloid leukemia cells. Leukemia 26: 1180-8.
- 607 12. Shen M, Bunaci R, Congleton J, Jensen H, Sayam L, et al. (2011) Interferon regu-
608 latory factor-1 binds c-Cbl, enhances mitogen activated protein kinase signaling and
609 promotes retinoic acid-induced differentiation of HL-60 human myelo-monoblastic
610 leukemia cells. Leuk Lymphoma 52: 2372-9.
- 611 13. Shen M, Yen A (2009) c-Cbl tyrosine kinase-binding domain mutant G306E abol-
612 ishes the interaction of c-Cbl with CD38 and fails to promote retinoic acid-induced
613 cell differentiation and G0 arrest. J Biol Chem 284: 25664–25677.
- 614 14. Yen A, Varvayanis S, Smith J, Lamkin T (2006) Retinoic acid induces expression of
615 SLP-76: expression with c-FMS enhances ERK activation and retinoic acid-induced
616 differentiation/G0 arrest of HL-60 cells. Eur J Cell Biol 85: 117–132.
- 617 15. Marchisio M, Bertagnolo V, Colamussi ML, Capitani S, Neri LM (1998) Phos-
618 phatidylinositol 3-kinase in HL-60 nuclei is bound to the nuclear matrix and increases
619 during granulocytic differentiation. Biochem Biophys Res Commun 253: 346-51.
- 620 16. Congleton J, Jiang H, Malavasi F, Lin H, Yen A (2011) ATRA-induced HL-60 myeloid
621 leukemia cell differentiation depends on the CD38 cytosolic tail needed for mem-
622 brane localization, but CD38 enzymatic activity is unnecessary. Exp Cell Res 317:
623 910–919.
- 624 17. Wang J, Yen A (2004) A novel retinoic acid-responsive element regulates retinoic
625 acid induced BLR1 expression. Mol Cell Biol 24: 2423 - 2443.
- 626 18. Yen A (1990) HL-60 cells as a model of growth and differentiation: the significance
627 of variant cells. Hematology Review 4: 5-46.
- 628 19. Yang T, Xiong Q, Enslen H, Davis R, Chow CW (2002) Phosphorylation of NFATc4
629 by p38 mitogen-activated protein kinases. Mol Cell Biol 22: 3892–3904.

- 630 20. Wang J, Yen A (2008) A MAPK-positive Feedback Mechanism for BLR1 Signaling
631 Propels Retinoic Acid-triggered Differentiation and Cell Cycle Arrest. *J Biol Chem*
632 283: 4375–4386.
- 633 21. Tasseff R, Nayak S, Song S, Yen A, Varner J (2011) Modeling and analysis of retinoic
634 acid induced differentiation of uncommitted precursor cells. *Integr Biol* 3: 578 - 591.
- 635 22. Jensen HA, Styskal LE, Tasseff R, Bunaciu RP, Congleton J, et al. (2013) The
636 src-family kinase inhibitor pp2 rescues inducible differentiation events in emergent
637 retinoic acid-resistant myeloblastic leukemia cells. *PLoS One* 8: e58621.
- 638 23. Jensen HA, Bunaciu RP, Ibabao CN, Myers R, Varner JD, et al. (2014) Retinoic acid
639 therapy resistance progresses from unilineage to bilineage in hl-60 leukemic blasts.
640 *PLoS One* 9: e98929.
- 641 24. Jensen HA, Bunaciu RP, Varner JD, Yen A (2015) Gw5074 and pp2 kinase inhibitors
642 implicate nontraditional c-raf and lyn function as drivers of retinoic acid-induced mat-
643 uration. *Cell Signal* 27: 1666-75.
- 644 25. Jensen HA, Yourish HB, Bunaciu RP, Varner JD, Yen A (2015) Induced myelomono-
645 cytic differentiation in leukemia cells is accompanied by noncanonical transcription
646 factor expression. *FEBS Open Bio* 5: 789-800.
- 647 26. Milo R, Jorgensen P, Moran U, Weber G, Springer M (2010) Bionumbers—the
648 database of key numbers in molecular and cell biology. *Nucleic Acids Res* 38: D750-
649 3.
- 650 27. Katagiri K, Hattori S, Nakamura S, Yamamoto T, Yoshida T, et al. (1994) Activation
651 of ras and formation of gap complex during tpa-induced monocytic differentiation of
652 hl-60 cells. *Blood* 84: 1780–1789.
- 653 28. Miranda MB, Johnson DE (2007) Signal transduction pathways that contribute to
654 myeloid differentiation. *Leukemia* 21: 1363–1377.
- 655 29. Hickstein DD, Back AL, Collins SJ (1989) Regulation of expression of the cd11b and

- 656 cd18 subunits of the neutrophil adherence receptor during human myeloid differen-
657 tiation. *J Biol Chem* 264: 21812–21817.
- 658 30. Hornstein I, Alcover A, Katzav S (2004) Vav proteins, masters of the world of cy-
659 toskeleton organization. *Cell Signal* 16: 1-11.
- 660 31. Ferrell J (2002) Self-perpetuating states in signal transduction: positive feedback,
661 double-negative feedback and bistability. *Curr Opin Cell Biol* 14: 140-8.
- 662 32. Laslo P, Spooner CJ, Warmflash A, Lancki DW, Lee HJ, et al. (2006) Multilineage
663 transcriptional priming and determination of alternate hematopoietic cell fates. *Cell*
664 126: 755-66.
- 665 33. Xiong W, Ferrell J (2003) A positive-feedback-based bistable 'memory module' that
666 governs a cell fate decision. *Nature* 426: 460-5.
- 667 34. Bagci EZ, Vodovotz Y, Billiar TR, Ermentrout GB, Bahar I (2006) Bistability in apop-
668 tosis: roles of bax, bcl-2, and mitochondrial permeability transition pores. *Biophys J*
669 90: 1546-59.
- 670 35. Luan D, Zai M, Varner JD (2007) Computationally derived points of fragility of a
671 human cascade are consistent with current therapeutic strategies. *PLoS Comput*
672 *Biol* 3: e142.
- 673 36. Friedman AD (2007) Transcriptional control of granulocyte and monocyte develop-
674 ment. *Oncogene* 26: 6816-28.
- 675 37. Dahl R, Walsh JC, Lancki D, Laslo P, Iyer SR, et al. (2003) Regulation of macrophage
676 and neutrophil cell fates by the PU.1:C/EBPalpha ratio and granulocyte colony-
677 stimulating factor. *Nat Immunol* 4: 1029-36.
- 678 38. El-Benna J, Dang PMC, Gougerot-Pocidalo MA, Marie JC, Braut-Boucher F (2009)
679 p47phox, the phagocyte nadph oxidase/nox2 organizer: structure, phosphorylation
680 and implication in diseases. *Exp Mol Med* 41: 217-25.
- 681 39. Cleghon V, Morrison DK (1994) Raf-1 interacts with fyn and src in a non-

- 682 phosphotyrosine-dependent manner. *J Biol Chem* 269: 17749–17755.
- 683 40. Zimmermann S, Moelling K (1999) Phosphorylation and regulation of raf by akt (pro-
684 tein kinase b). *Science* 286: 1741–1744.
- 685 41. Ritt DA, Zhou M, Conrads TP, Veenstra TD, Copeland TD, et al. (2007) Ck2 is a
686 component of the ksr1 scaffold complex that contributes to raf kinase activation.
687 *Curr Biol* 17: 179–184.
- 688 42. Hekman M, Wiese S, Metz R, Albert S, Troppmair J, et al. (2004) Dynamic changes
689 in c-raf phosphorylation and 14-3-3 protein binding in response to growth factor stim-
690 ulation: differential roles of 14-3-3 protein binding sites. *J Biol Chem* 279: 14074–
691 14086.
- 692 43. Dhillon AS, Yip YY, Grindlay GJ, Pakay JL, Dangers M, et al. (2009) The c-terminus
693 of raf-1 acts as a 14-3-3-dependent activation switch. *Cell Signal* 21: 1645–1651.
- 694 44. Song JS, Gomez J, Stancato LF, Rivera J (1996) Association of a p95 vav-containing
695 signaling complex with the fcepsilonri gamma chain in the rbl-2h3 mast cell line.
696 evidence for a constitutive in vivo association of vav with grb2, raf-1, and erk2 in an
697 active complex. *J Biol Chem* 271: 26962–26970.
- 698 45. Costello PS, Walters AE, Mee PJ, Turner M, Reynolds LF, et al. (1999) The rho-
699 family gtp exchange factor vav is a critical transducer of t cell receptor signals to the
700 calcium, erk, and nf-kappab pathways. *Proc Natl Acad Sci U S A* 96: 3035–3040.
- 701 46. Graham D, Robertson C, Bautista J, Mascarenhas F, Diacovo M, et al. (2007)
702 Neutrophil-mediated oxidative burst and host defense are controlled by a Vav-
703 PLCgamma2 signaling axis in mice. *J Clin Invest* 117: 3445–3452.
- 704 47. Kim HS, Lim IK (2009) Phosphorylated extracellular signal-regulated protein kinases
705 1 and 2 phosphorylate sp1 on serine 59 and regulate cellular senescence via tran-
706 scription of p21sdi1/cip1/waf1. *J Biol Chem* 284: 15475–15486.
- 707 48. Milanini-Mongiat J, Pouyss?gur J, Pag?e G (2002) Identification of two sp1 phos-

- 708 phosphorylation sites for p42/p44 mitogen-activated protein kinases: their implication in
709 vascular endothelial growth factor gene transcription. *J Biol Chem* 277: 20631–
710 20639.
- 711 49. Zhang Y, Cho YY, Petersen BL, Zhu F, Dong Z (2004) Evidence of stat1 phosphory-
712 lation modulated by mapks, mek1 and msk1. *Carcinogenesis* 25: 1165–1175.
- 713 50. Li Z, Theus MH, Wei L (2006) Role of erk 1/2 signaling in neuronal differentiation of
714 cultured embryonic stem cells. *Dev Growth Differ* 48: 513–523.
- 715 51. Yen A, Reece SL, Albright KL (1984) Dependence of hl-60 myeloid cell differentiation
716 on continuous and split retinoic acid exposures: precommitment memory associated
717 with altered nuclear structure. *J Cell Physiol* 118: 277–286.
- 718 52. Moon TS, Lou C, Tamsir A, Stanton BC, Voigt CA (2012) Genetic programs con-
719 structed from layered logic gates in single cells. *Nature* 491: 249-53.
- 720 53. Wayman JA, Sagar A, Varner JD (2015) Dynamic modeling of cell-free biochemical
721 networks using effective kinetic models. *Processes* 3: 138.
- 722 54. Igel C, Hansen N, Roth S (2007) Covariance matrix adaptation for multi-objective
723 optimization. *Evol Comput* 15: 1-28.
- 724 55. Bezanson J, Edelman A, Karpinski S, Shah VB (2014) Julia: A fresh approach to
725 numerical computing. *CoRR* abs/1411.1607.
- 726 56. Brooks SC, Kazmer S, Levin AA, Yen A (1996) Myeloid differentiation and retinoblas-
727 toma phosphorylation changes in HL-60 cells induced by retinoic acid receptor- and
728 retinoid X receptor-selective retinoic acid analogs. *Blood* 87: 227–237.
- 729 57. Rishi AK, Gerald TM, Shao ZM, Li XS, Baumann RG, et al. (1996) Regulation of the
730 human retinoic acid receptor alpha gene in the estrogen receptor negative human
731 breast carcinoma cell lines skbr-3 and mda-mb-435. *Cancer Res* 56: 5246-52.
- 732 58. Mueller BU, Pabst T, Fos J, Petkovic V, Fey MF, et al. (2006) Atra resolves the dif-
733 ferentiation block in t(15;17) acute myeloid leukemia by restoring pu.1 expression.

- 734 Blood 107: 3330-8.
- 735 59. Luo XM, Ross AC (2006) Retinoic acid exerts dual regulatory actions on the ex-
736 pression and nuclear localization of interferon regulatory factor-1. *Exp Biol Med*
737 (Maywood) 231: 619-31.
- 738 60. Sylvester I, Schöler HR (1994) Regulation of the oct-4 gene by nuclear receptors.
739 *Nucleic Acids Res* 22: 901-11.
- 740 61. Drach J, McQueen T, Engel H, Andreeff M, Robertson KA, et al. (1994) Retinoic
741 acid-induced expression of cd38 antigen in myeloid cells is mediated through
742 retinoic acid receptor-alpha. *Cancer Res* 54: 1746-52.
- 743 62. Liu M, Iavarone A, Freedman LP (1996) Transcriptional activation of the human
744 p21(waf1/cip1) gene by retinoic acid receptor. correlation with retinoid induction of
745 u937 cell differentiation. *J Biol Chem* 271: 31723-8.
- 746 63. Bunaciu RP, Yen A (2013) 6-formylindolo (3,2-b)carbazole (ficz) enhances retinoic
747 acid (ra)-induced differentiation of hl-60 myeloblastic leukemia cells. *Mol Cancer* 12:
748 39.
- 749 64. Balmer JE, Blomhoff R (2002) Gene expression regulation by retinoic acid. *J Lipid*
750 *Res* 43: 1773-808.
- 751 65. Rosen ED, Hsu CH, Wang X, Sakai S, Freeman MW, et al. (2002) C/ebpalpha in-
752 duces adipogenesis through ppargamma: a unified pathway. *Genes Dev* 16: 22-6.
- 753 66. Varley CL, Bacon EJ, Holder JC, Southgate J (2009) Foxa1 and irf-1 intermediary
754 transcriptional regulators of ppargamma-induced urothelial cytodifferentiation. *Cell*
755 *Death Differ* 16: 103-14.
- 756 67. Bruemmer D, Yin F, Liu J, Berger JP, Sakai T, et al. (2003) Regulation of the growth
757 arrest and dna damage-inducible gene 45 (gadd45) by peroxisome proliferator-
758 activated receptor gamma in vascular smooth muscle cells. *Circ Res* 93: e38-47.
- 759 68. Delerive P, De Bosscher K, Besnard S, Vanden Berghe W, Peters JM, et al. (1999)

- 760 PEROXISOME PROLIFERATOR-ACTIVATED RECEPTOR ALPHA NEGATIVELY REGULATES THE VASCULAR
761 INFLAMMATORY GENE RESPONSE BY NEGATIVE CROSS-TALK WITH TRANSCRIPTION FACTORS NF-
762 KAPPAB AND AP-1. J BIOL CHEM 274: 32048-54.
- 763 69. Altiok S, Xu M, Spiegelman BM (1997) Ppargamma induces cell cycle withdrawal:
764 inhibition of e2f/dp dna-binding activity via down-regulation of pp2a. GENES DEV 11:
765 1987-98.
- 766 70. Fei J, Cook C, Gillespie M, Yu B, Fullen K, et al. (2011) Atherogenic ω -6 lipids mod-
767 ulate ppar- egr-1 crosstalk in vascular cells. PPAR RES 2011: 753917.
- 768 71. Song EK, Lee YR, Kim YR, Yeom JH, Yoo CH, et al. (2012) Naadp mediates insulin-
769 stimulated glucose uptake and insulin sensitization by ppar γ in adipocytes. CELL REP
770 2: 1607-19.
- 771 72. Szanto A, Nagy L (2005) Retinoids potentiate peroxisome proliferator-activated re-
772 ceptor gamma action in differentiation, gene expression, and lipid metabolic pro-
773 cesses in developing myeloid cells. Mol Pharmacol 67: 1935-43.
- 774 73. Han S, Sidell N, Fisher PB, Roman J (2004) Up-regulation of p21 gene expres-
775 sion by peroxisome proliferator-activated receptor gamma in human lung carcinoma
776 cells. Clin Cancer Res 10: 1911-9.
- 777 74. Von Knethen A, Brüne B (2002) Activation of peroxisome proliferator-activated re-
778 ceptor gamma by nitric oxide in monocytes/macrophages down-regulates p47phox
779 and attenuates the respiratory burst. J Immunol 169: 2619-26.
- 780 75. Dispirito JR, Fang B, Wang F, Lazar MA (2013) Pruning of the adipocyte peroxisome
781 proliferator-activated receptor γ cistrome by hematopoietic master regulator pu.1.
782 Mol Cell Biol 33: 3354-64.
- 783 76. Chen H, Ray-Gallet D, Zhang P, Hetherington CJ, Gonzalez DA, et al. (1995) Pu.1
784 (spi-1) autoregulates its expression in myeloid cells. Oncogene 11: 1549-60.
- 785 77. Steidl U, Rosenbauer F, Verhaak RGW, Gu X, Ebralidze A, et al. (2006) Essential

- 786 role of jun family transcription factors in pu.1 knockdown-induced leukemic stem
787 cells. Nat Genet 38: 1269-77.
- 788 78. Pahl HL, Scheibe RJ, Zhang DE, Chen HM, Galson DL, et al. (1993) The proto-
789 oncogene pu.1 regulates expression of the myeloid-specific cd11b promoter. J Biol
790 Chem 268: 5014-20.
- 791 79. Yuki H, Ueno S, Tatetsu H, Niiro H, Iino T, et al. (2013) Pu.1 is a potent tumor
792 suppressor in classical hodgkin lymphoma cells. Blood 121: 962-70.
- 793 80. Li SL, Schlegel W, Valente AJ, Clark RA (1999) Critical flanking sequences of pu.1
794 binding sites in myeloid-specific promoters. J Biol Chem 274: 32453-60.
- 795 81. Timchenko N, Wilson DR, Taylor LR, Abdelsayed S, Wilde M, et al. (1995) Autoreg-
796 ulation of the human c/ebp alpha gene by stimulation of upstream stimulatory factor
797 binding. Mol Cell Biol 15: 1192-202.
- 798 82. Lidonnici MR, Audia A, Soliera AR, Prisco M, Ferrari-Amorotti G, et al. (2010) Ex-
799 pression of the transcriptional repressor gfi-1 is regulated by c/ebpalpha and is
800 involved in its proliferation and colony formation-inhibitory effects in p210bcr/abl-
801 expressing cells. Cancer Res 70: 7949-59.
- 802 83. D'Alo' F, Johansen LM, Nelson EA, Radomska HS, Evans EK, et al. (2003) The
803 amino terminal and e2f interaction domains are critical for c/ebp alpha-mediated
804 induction of granulopoietic development of hematopoietic cells. Blood 102: 3163-
805 71.
- 806 84. Pan Z, Hetherington CJ, Zhang DE (1999) Ccaat/enhancer-binding protein activates
807 the cd14 promoter and mediates transforming growth factor beta signaling in mono-
808 cyte development. J Biol Chem 274: 23242-8.
- 809 85. Harris TE, Albrecht JH, Nakanishi M, Darlington GJ (2001) Ccaat/enhancer-binding
810 protein-alpha cooperates with p21 to inhibit cyclin-dependent kinase-2 activity and
811 induces growth arrest independent of dna binding. J Biol Chem 276: 29200-9.

- 812 86. Bauvois B, Durant L, Laboureau J, Barthélémy E, Rouillard D, et al. (1999) Upreg-
813 ulation of cd38 gene expression in leukemic b cells by interferon types i and ii. *J*
814 *Interferon Cytokine Res* 19: 1059-66.
- 815 87. Passioura T, Dolnikov A, Shen S, Symonds G (2005) N-ras-induced growth suppres-
816 sion of myeloid cells is mediated by irf-1. *Cancer Res* 65: 797-804.
- 817 88. Dahl R, Iyer SR, Owens KS, Cuylear DD, Simon MC (2007) The transcriptional
818 repressor gfi-1 antagonizes pu.1 activity through protein-protein interaction. *J Biol*
819 *Chem* 282: 6473-83.
- 820 89. Duan Z, Horwitz M (2003) Targets of the transcriptional repressor oncoprotein gfi-1.
821 *Proc Natl Acad Sci U S A* 100: 5932-7.
- 822 90. Chen H, Zhang P, Radomska HS, Hetherington CJ, Zhang DE, et al. (1996) Octamer
823 binding factors and their coactivator can activate the murine pu.1 (spi-1) promoter.
824 *J Biol Chem* 271: 15743-52.
- 825 91. Behre G, Whitmarsh AJ, Coghan MP, Hoang T, Carpenter CL, et al. (1999) c-jun
826 is a jnk-independent coactivator of the pu.1 transcription factor. *J Biol Chem* 274:
827 4939-46.
- 828 92. Kardassis D, Papakosta P, Pardali K, Moustakas A (1999) c-jun transactivates the
829 promoter of the human p21(waf1/cip1) gene by acting as a superactivator of the
830 ubiquitous transcription factor sp1. *J Biol Chem* 274: 29572-81.
- 831 93. Johnson DG, Ohtani K, Nevins JR (1994) Autoregulatory control of e2f1 expression
832 in response to positive and negative regulators of cell cycle progression. *Genes Dev*
833 8: 1514-25.
- 834 94. Fu M, Zhang J, Lin Y, Zhu X, Ehrengruber MU, et al. (2002) Early growth response
835 factor-1 is a critical transcriptional mediator of peroxisome proliferator-activated
836 receptor-gamma 1 gene expression in human aortic smooth muscle cells. *J Biol*
837 *Chem* 277: 26808-14.

- 838 95. Mak KS, Funnell APW, Pearson RCM, Crossley M (2011) Pu.1 and haematopoietic
839 cell fate: Dosage matters. *Int J Cell Biol* 2011: 808524.
- 840 96. Chen F, Wang Q, Wang X, Studzinski GP (2004) Up-regulation of egr1 by 1,25-
841 dihydroxyvitamin d3 contributes to increased expression of p35 activator of cyclin-
842 dependent kinase 5 and consequent onset of the terminal phase of hl60 cell differ-
843 entiation. *Cancer Res* 64: 5425-33.
- 844 97. Suh J, Jeon YJ, Kim HM, Kang JS, Kaminski NE, et al. (2002) Aryl hydrocarbon
845 receptor-dependent inhibition of ap-1 activity by 2,3,7,8-tetrachlorodibenzo-p-dioxin
846 in activated b cells. *Toxicol Appl Pharmacol* 181: 116-23.
- 847 98. Shen M, Bunaciu RP, Congleton J, Jensen HA, Sayam LG, et al. (2011) Inter-
848 feron regulatory factor-1 binds c-cbl, enhances mitogen activated protein kinase
849 signaling and promotes retinoic acid-induced differentiation of hl-60 human myelo-
850 monoblastic leukemia cells. *Leuk Lymphoma* 52: 2372-9.
- 851 99. Bunaciu RP, Yen A (2011) Activation of the aryl hydrocarbon receptor ahr promotes
852 retinoic acid-induced differentiation of myeloblastic leukemia cells by restricting ex-
853 pression of the stem cell transcription factor oct4. *Cancer Res* 71: 2371-80.
- 854 100. Jackson DA, Pombo A, Iborra F (2000) The balance sheet for transcription: an anal-
855 ysis of nuclear rna metabolism in mammalian cells. *FASEB J* 14: 242-54.
- 856 101. Zhao ZW, Roy R, Gebhardt JCM, Suter DM, Chapman AR, et al. (2014) Spatial orga-
857 nization of rna polymerase ii inside a mammalian cell nucleus revealed by reflected
858 light-sheet superresolution microscopy. *Proc Natl Acad Sci U S A* 111: 681-6.
- 859 102. Freitas R, Merkle R (2004) Kinematic Self-Replicating Machines. Oxford University
860 Press.
- 861 103. Yang E, van Nimwegen E, Zavolan M, Rajewsky N, Schroeder M, et al. (2003) De-
862 cay rates of human mrnas: correlation with functional characteristics and sequence
863 attributes. *Genome Res* 13: 1863-72.

- 864 104. Doherty MK, Hammond DE, Clague MJ, Gaskell SJ, Beynon RJ (2009) Turnover
865 of the human proteome: determination of protein intracellular stability by dynamic
866 silac. *J Proteome Res* 8: 104-12.
- 867 105. Sehgal PB, Derman E, Molloy GR, Tamm I, Darnell JE (1976) 5,6-dichloro-1-beta-
868 d-ribofuranosylbenzimidazole inhibits initiation of nuclear heterogeneous rna chains
869 in hela cells. *Science* 194: 431-3.
- 870 106. Darzacq X, Shav-Tal Y, de Turris V, Brody Y, Shenoy SM, et al. (2007) In vivo dy-
871 namics of rna polymerase ii transcription. *Nat Struct Mol Biol* 14: 796-806.
- 872 107. Kos M, Tollervey D (2010) Yeast pre-rrna processing and modification occur cotran-
873 scriptionally. *Mol Cell* 37: 809-20.
- 874 108. Darnell JE Jr (2013) Reflections on the history of pre-mrna processing and highlights
875 of current knowledge: a unified picture. *RNA* 19: 443-60.
- 876 109. Boström K, Wettsten M, Borén J, Bondjers G, Wiklund O, et al. (1986) Pulse-chase
877 studies of the synthesis and intracellular transport of apolipoprotein b-100 in hep g2
878 cells. *J Biol Chem* 261: 13800-6.
- 879 110. Meyers R, editor (2004) *Encyclopedia of Molecular Cell Biology and Molecular*
880 *Medicine*, Volume 1, 2nd Edition. ISBN: 978-3-527-30543-8. Wiley-Blackwell.
- 881 111. Rosenbluth MJ, Lam WA, Fletcher DA (2006) Force microscopy of nonadherent
882 cells: a comparison of leukemia cell deformability. *Biophys J* 90: 2994-3003.

Table 1: Myelomonocytic transcription factor connectivity used in the signal integration and phenotype modules.

883

884

Effector	Effect	Target	Source
RAR α	+	RAR α	(57)
	+	PU.1	(58)
	+	C/EBP α	(36)
	+	IRF-1	(59)
	-	Oct4	(60)
	+	CD38	(61)
	+	p21	(62)
	+	AhR	(63)
	+	EGR1	(64)
PPAR γ	+	C/EBP α	(65)
	+	IRF-1	(66)
	+	Oct1	(67)
	-	AP-1	(68)
	-	E2F	(69)
	-	EGR1	(70)
	+	CD38	(71)
	+	CD14	(72)
	+	p21	(73)
	-	p47phox	(74)
PU.1	-	PPAR γ	(75)
	+	PU.1	(76)
	+	AP-1	(77)
	+	EGR1	(32)
	+	CD11b	(78)
	+	p21	(79)
	+	p47phox	(80)
C/EBP α	+	PPAR γ	(65)
	+	PU.1	(37)
	+	C/EBP α	(81)
	+	Gfi-1	(82)
	-	E2F	(83)
	+	CD14	(84)

	+	p21	(85)
IRF-1	+	CD38	(86)
	+	p21	(87)
	-	PU.1	(88)
	-	C/EBP α	(89)
	-	E2F	(89)
	-	EGR1	(32)
	-	p21	(89)
Oct1	+	PU.1	(90)
AP-1	-	PPAR γ	(68)
	+	PU.1	(91)
	+	p21	(92)
E2F	+	E2F	(93)
EGR1	+	PPAR γ	(94)
	-	Gfi-1	(95)
	+	CD14	(96)
AhR	+	AP-1	(97)
	+	IRF-1	(98)
	-	Oct4	(99)
	-	PU.1	

Table 2: Characteristic model parameters estimated from literature.

Symbol	Description	Value	Units	Source
R_1	RNA polymerase abundance	85,000	copies/cell	(100, 101)
R_2	Ribosome abundance	1×10^6	copies/cell	(102)
G_i	Characteristic gene abundance	2	copies/cell	this study
K_X	Saturation constant transcription	600	copies/cell	this study
K_T	Saturation constant translation	95,000	copies/cell	this study
$t_{1/2,m}$	characteristic mRNA half-life (transcription factor)	2-4	hr	(103)
$t_{1/2,p}$	characteristic protein half-life	10	hr	(104)
$\theta_{m,j}$	characteristic mRNA degradation constant	0.34	hr^{-1}	derived
$\theta_{p,j}$	characteristic protein degradation constant	0.07	hr^{-1}	derived
887				
t_d	HL-60 doubling time	19.5	hr	this study
μ	growth rate	0.035	hr^{-1}	derived
k_d	death rate	0.10μ	hr^{-1}	derived
e_T	elongation rate RNA polymerase	50-100	nt/s	(105–108)
e_X	elongation rate Ribosome	5	aa/s	(109)
$L_{T,o}$	characteristic gene length	15,000	nt	(110)
$L_{X,o}$	characteristic transcript length	5,000	nt	derived
k_T	characteristic transcription rate	1.44	hr^{-1}	derived
k_X	characteristic translation rate	3.60	hr^{-1}	derived
D	Diameter of an HL-60 cell	12.4	μm^3	(111)
f_C	cytoplasmic fraction	0.51	dimensionless	(111)

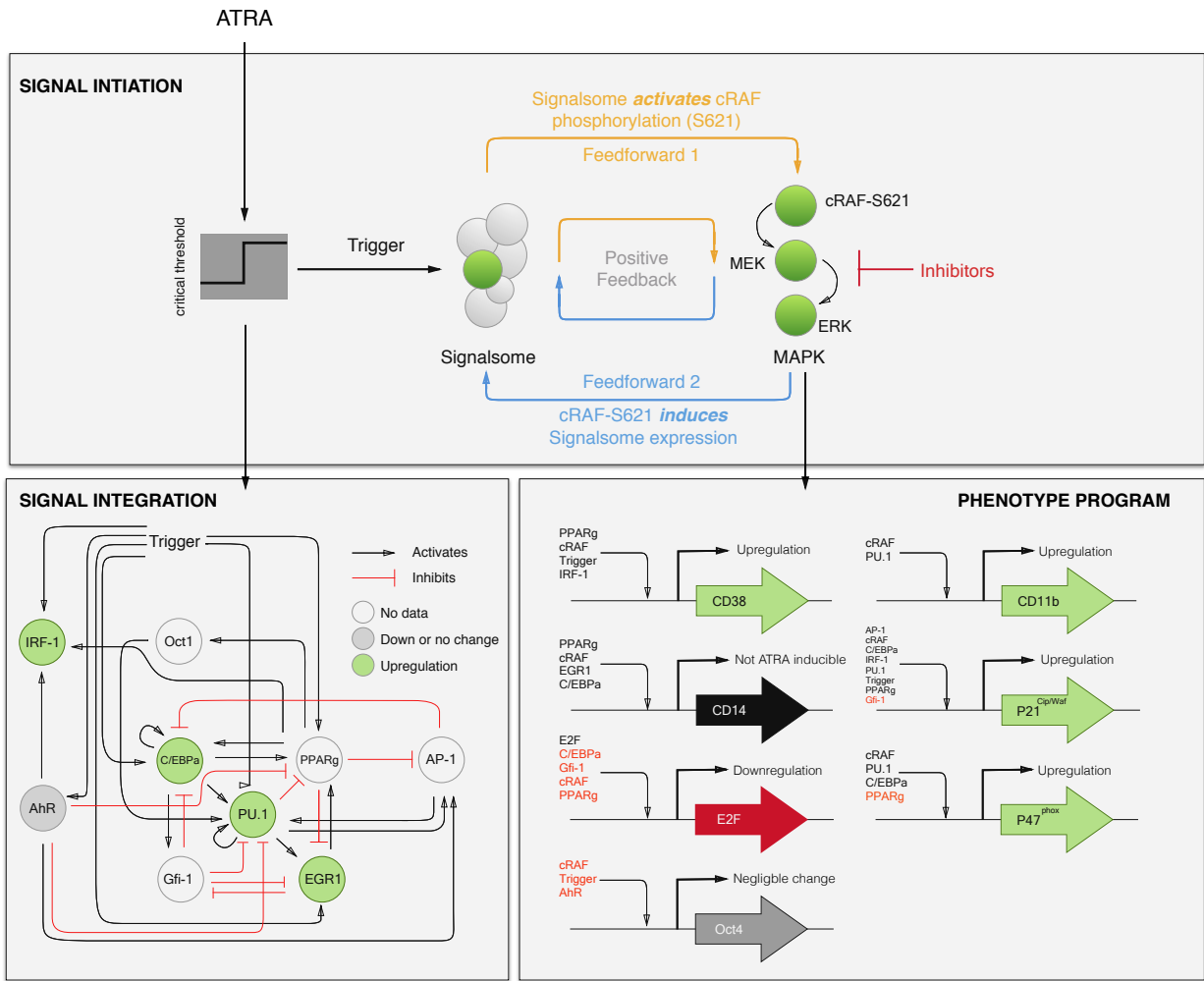


Fig. 1: Schematic of the effective ATRA differentiation circuit. Above a critical threshold, ATRA activates an upstream Trigger, which induces signalsome complex formation. Signalsome activates the mitogen-activated protein kinase (MAPK) cascade which in turn drives the differentiation program and signalsome formation. Both Trigger and activated cRaf-pS621 drive a phenotype gene expression program responsible for differentiation. Trigger activates the expression of a series of transcription factors which in combination with cRaf-pS621 result in phenotypic change.

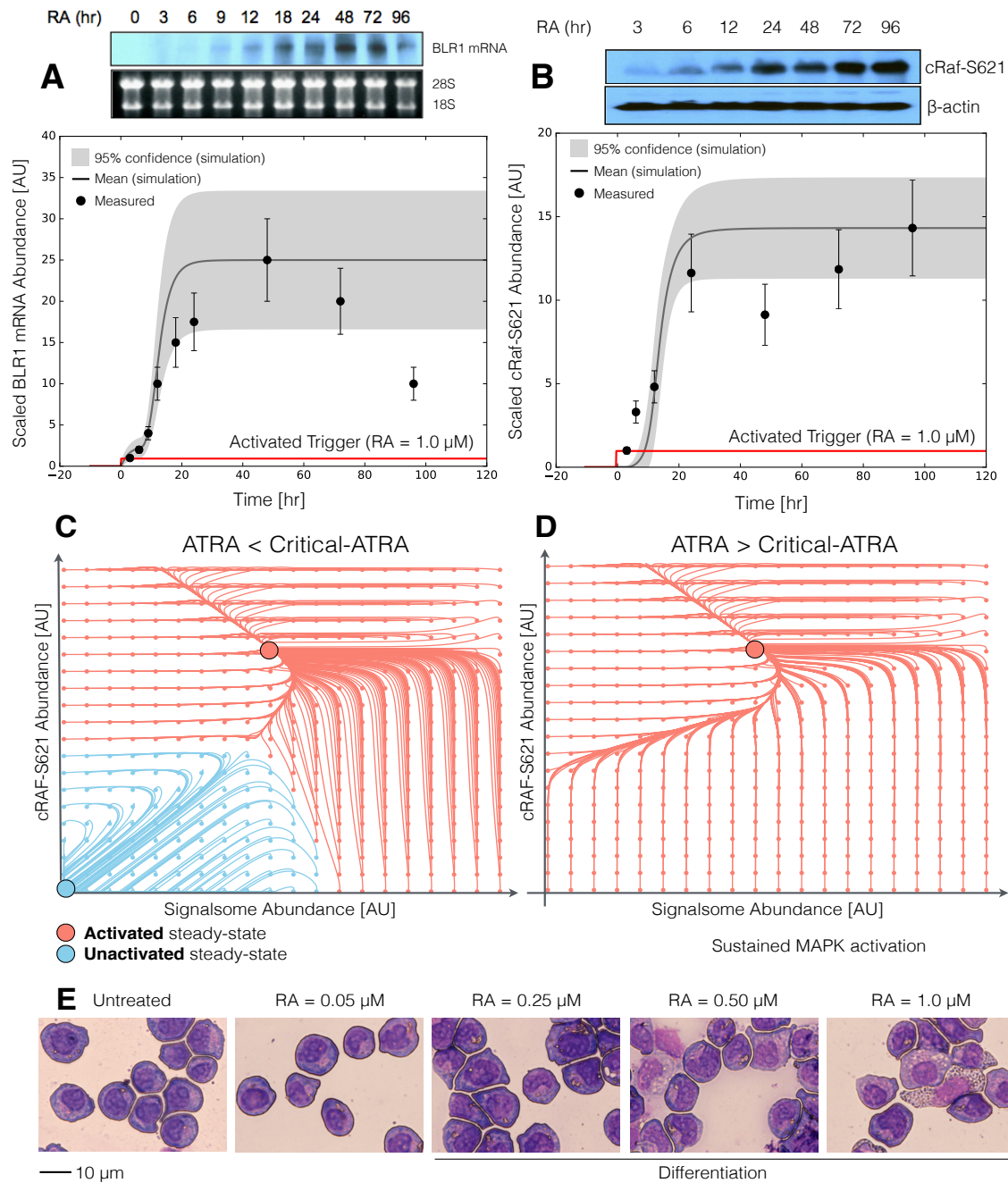


Fig. 2: Model analysis for ATRA-induced HL-60 differentiation. A: BLR1 mRNA versus time following exposure to $1\mu\text{M}$ ATRA at $t = 0$ hr. B: cRaf-pS621 versus time following exposure to $1\mu\text{M}$ ATRA at $t = 0$ hr. Points denote experimental measurements, solid lines denote the mean model performance. Shaded regions denote the 99% confidence interval calculated over the parameter ensemble. C: Signalsome and cRaf-pS621 nullclines for ATRA below the critical threshold. The model had two stable steady states and a single unstable state in this regime. D: Signalsome and cRaf-pS621 nullclines for ATRA above the critical threshold. In this regime the model had only a single stable steady state. E: Morphology of HL-60 as a function of ATRA concentration ($t = 72$ hr).

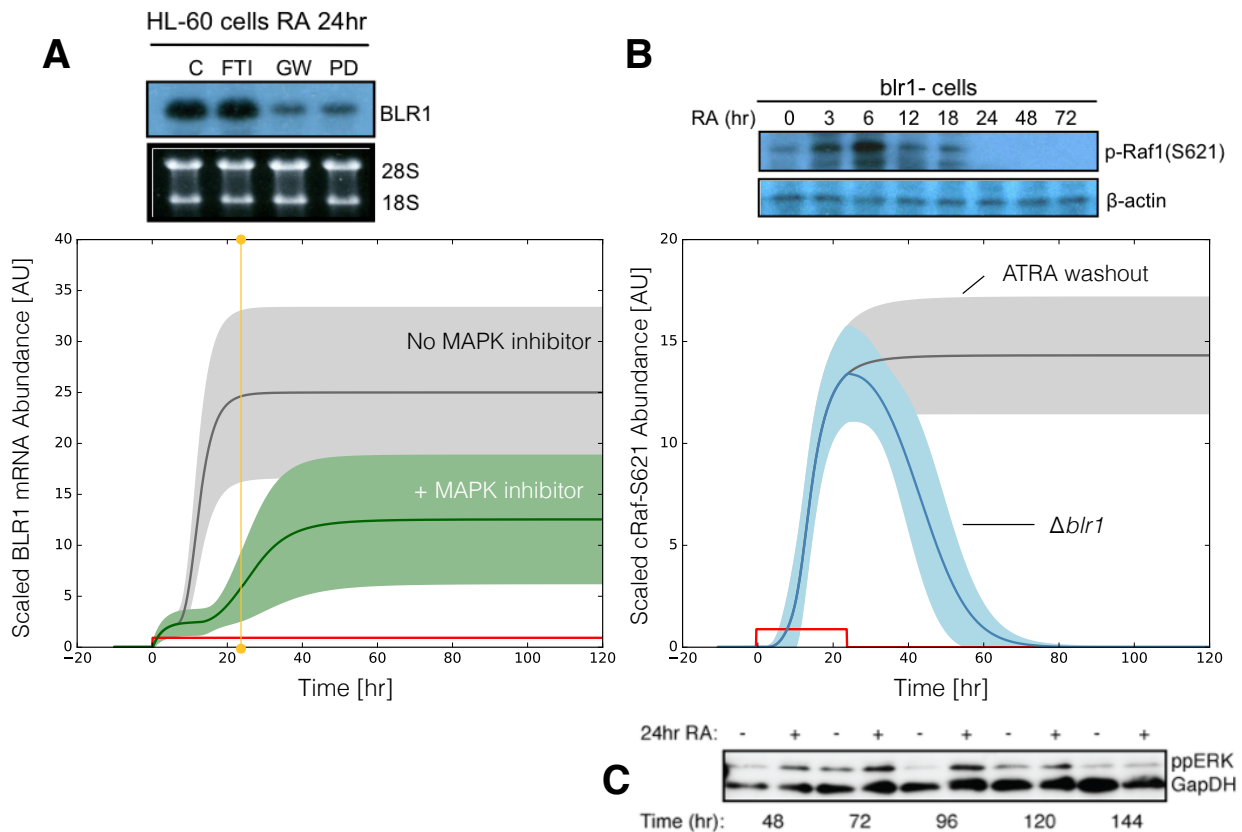


Fig. 3: Model simulation following exposure to $1\mu\text{M}$ ATRA. A: BLR1 mRNA versus time with and without MAPK inhibitor. B: cRaf-pS621 versus time following pulsed exposure to $1\mu\text{M}$ ATRA with and without BLR1. Solid lines denote the mean model performance, while shaded regions denote the 99% confidence interval calculated over the parameter ensemble. C: Western blot analysis of phosphorylated ERK1/2 in ATRA washout experiments. Experimental data in panels A and B were reproduced from Wang and Yen (20), data in panel C is reported in this study.

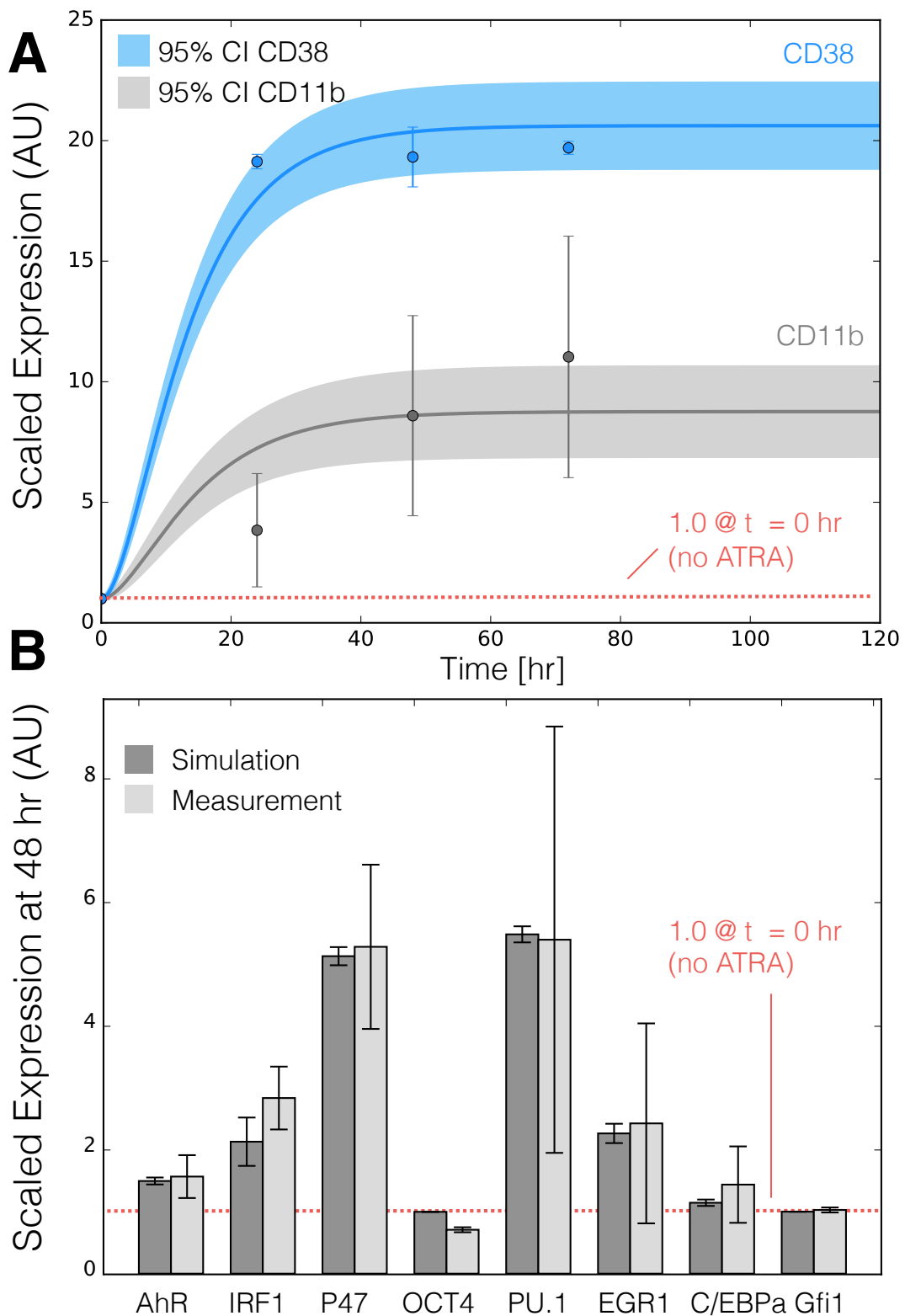


Fig. 4: Model simulation of the HL-60 gene expression program following exposure to $1\mu\text{M}$ ATRA at $t = 0$ hr. A: CD38 and CD11b expression versus time following ATRA exposure at time $t = 0$ hr. B: Gene expression at $t = 48$ hr following ATRA exposure. Experimental data in panels A and B were reproduced from Jensen et al. (25).

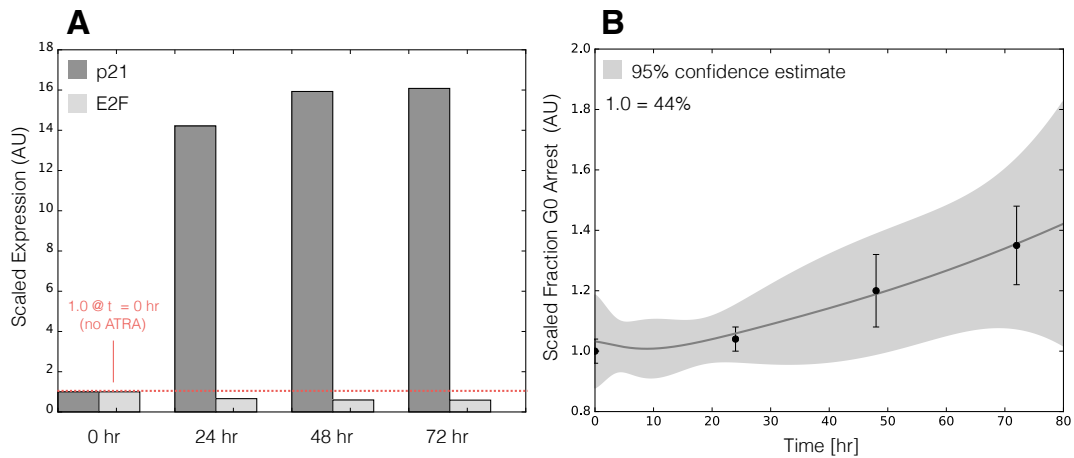


Fig. 5: Model simulation of HL-60 cell-cycle arrest following exposure to $1\mu\text{M}$ ATRA at $t = 0$ hr. A: Predicted p21 and E2F expression levels for the best parameter set following ATRA exposure at time $t = 0$ hr. B: Estimated fraction of HL-60 cells in G0 arrest following ATRA exposure at time $t = 0$ hr. The gray region denotes the 95% confidence estimate of the polynomial model. Experimental data in panel B was reproduced from Jensen et al. (25).

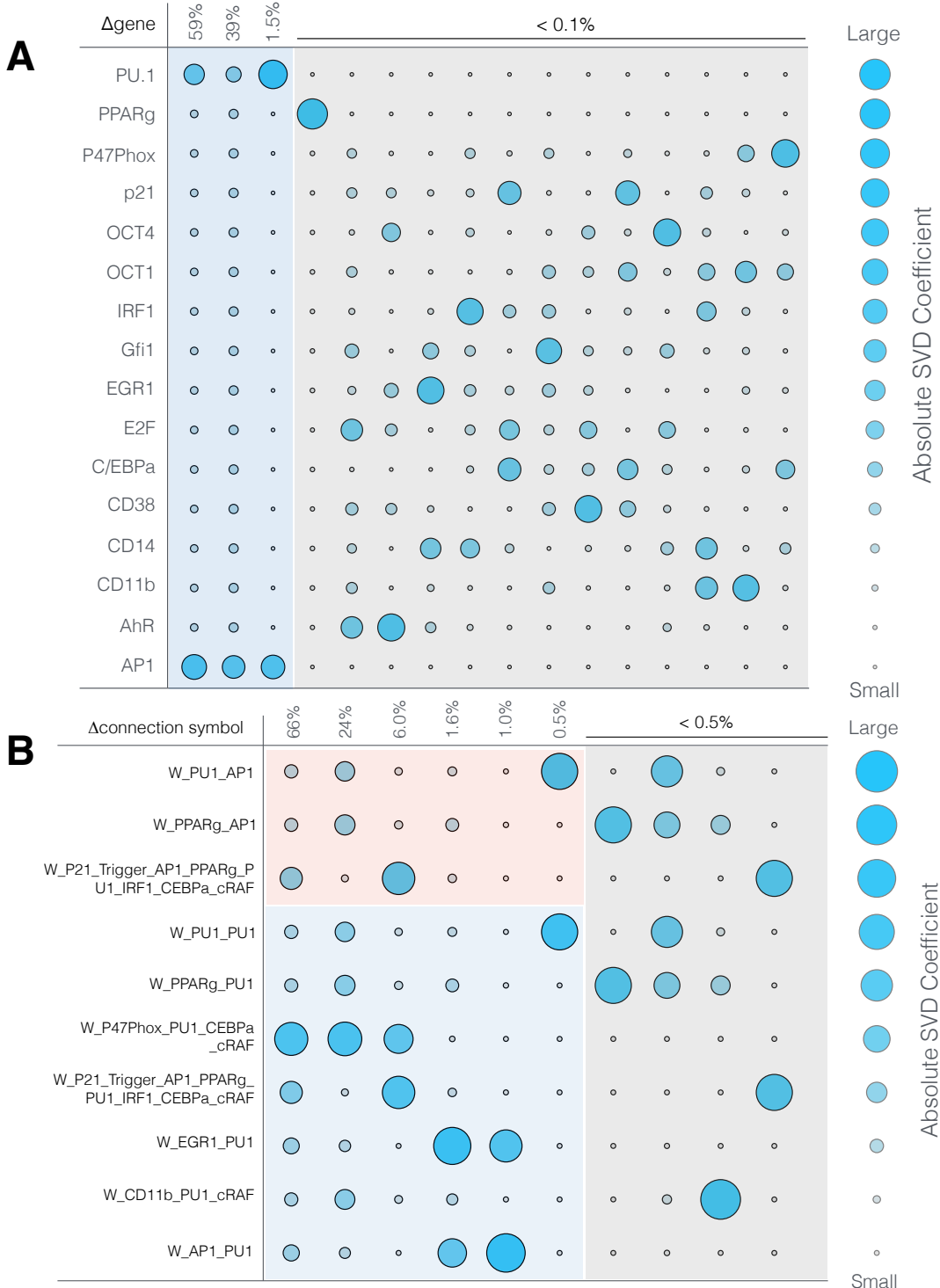


Fig. 6: Robustness of the HL-60 differentiation program following exposure to $1\mu\text{M}$ ATRA at $t = 0$ hr. A: Singular value decomposition of the system response (l^2 -norm between the perturbed and nominal state) following pairwise gene knockout simulations using the best fit parameter set. The percentage at the top of each column describes the fraction of the variance in the system state captured by the node combinations in the rows. B: Singular value decomposition of the system response (l^2 -norm between the perturbed and nominal state) following the pairwise removal of connections from the PU.1 and AP1 nodes.

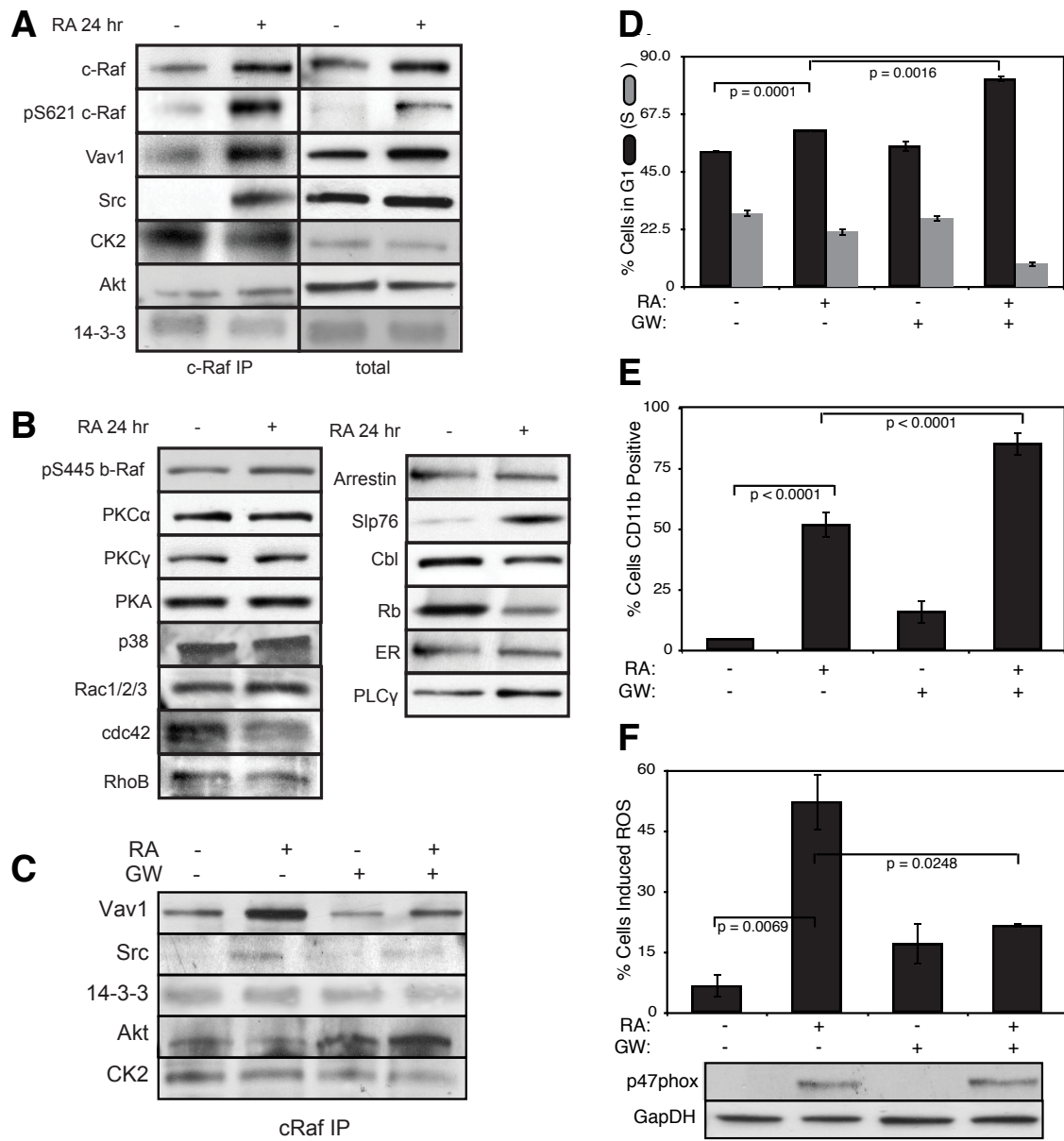


Fig. 7: Investigation of a panel of possible Raf interaction partners in the presence and absence of ATRA. A: Species identified to precipitate out with Raf: first column shows Western blot analysis on total Raf immunoprecipitation with and without 24 hr ATRA treatment and the second on total lysate. B: The expression of species considered that did not precipitate out with Raf at levels detectable by Western blot analysis on total lysate. C: Effect of the Raf inhibitor GW5074 on Raf interactions as determined by Western blot analysis of total Raf immunoprecipitation. The Authors note the signal associated with Src was found to be weak. D: Cell Cycle distribution as determined by flow cytometry indicated arrest induced by ATRA, which was increased by the addition of GW5074. E: Expression of the cell surface marker CD11b as determined by flow cytometry indicated increased expression induced by ATRA, which was enhanced by the addition of GW5074. F: Inducible reactive oxygen species (ROS) as determined by DCF flow cytometry. The functional differentiation response of ATRA treated cells was mitigated by GW5074.